

sonic waves may cause irreversible tissue injury. A minimum concentration of microbubbles would be desirable for clinical use. Optison has been used in the US and other countries for cardiac applications only, but it is not allowed for use in humans in some countries, such as Japan. Alternative clinical echo-contrast agents are now available in Japan. Levovist is one of these agents, although its gene transduction efficacy is reported to be inferior to that of Optison (27). Both are classified as second-generation microbubble agents. Optison consists of micrometer-sized (mean diameter 2–5 μm), denatured hollow albumin microspheres with a shell thickness of ~15 nm. The microbubbles are filled with octafluoropropane. Levovist is a galactose-based, air-filled microbubble agent, 99% of which is smaller than 7 μm . Further studies are planned to compare the performance of these agents in vivo.

This method can be used to introduce not only MTX but also other agents, such as steroids and some genes, into synovial cells. The procedure can be used not only for intraarticular injection but also for a systemic approach with intravenous or oral administration of the therapeutic drug. Studies are under way to examine these approaches. This technique enables a very targeted application of reagents to the diseased tissue, thus enabling healthy tissue to be spared from treatment.

REFERENCES

- Hall GH, Jones BI, Head AC, Jones VE. Intra-articular methotrexate: clinical and laboratory study in rheumatoid and psoriatic arthritis. *Ann Rheum Dis* 1978;37:351–6.
- Marks JS, Stewart IM, Hunter JA. Intra-articular methotrexate in rheumatoid arthritis [letter]. *Lancet* 1976;2:857–8.
- Franchi F, Seminara P, Codacci-Pisanelli G, Aronne T, Avella A, Bonomo L. Intra-articular methotrexate in the therapy of rheumatoid arthritis. *Recenti Prog Med* 1989;80:261–2.
- Bertino JR, Goker E, Gorlick R, Li WW, Banerjee D. Resistance mechanisms to methotrexate in tumors [review]. *Stem Cells* 1996;14:5–9.
- Nakashima-Matsushita N, Homma T, Yu S, Matsuda T, Sunahara N, Nakamura T, et al. Selective expression of folate receptor β and its possible role in methotrexate transport in synovial macrophages from patients with rheumatoid arthritis. *Arthritis Rheum* 1999;42:1609–16.
- Ifergan I, Meller I, Issakov J, Assaraf YG. Reduced folate carrier protein expression in osteosarcoma: implications for the prediction of tumor chemosensitivity. *Cancer* 2003;98:1958–66.
- Tachibana K, Uchida T, Ogawa K, Yamashita N, Tamura K. Induction of cell-membrane porosity by ultrasound [letter]. *Lancet* 1999;353:1409.
- Kim HJ, Greenleaf JF, Kinnick RR, Bronk JT, Bolander ME. Ultrasound-mediated transfection of mammalian cells. *Hum Gene Ther* 1996;7:1339–46.
- Ohta S, Suzuki K, Tachibana K, Yamada G. Microbubble-enhanced sonoporation: efficient gene transduction technique for chick embryos. *Genesis* 2003;37:91–101.
- Hashiya N, Aoki M, Tachibana K, Taniyama Y, Yamasaki K, Hiraoka K, et al. Local delivery of E2F decoy oligodeoxynucleotides using ultrasound with microbubble agent (Optison) inhibits intimal hyperplasia after balloon injury in rat carotid artery model. *Biochem Biophys Res Commun* 2004;317:508–14.
- Yamasaki K, Asai T, Shimizu M, Aoki M, Hashiya N, Sakonjo H, et al. Inhibition of NF κ B activation using cis-element 'decoy' of NF κ B binding site reduces neointimal formation in porcine balloon-injured coronary artery model. *Gene Ther* 2003;10:356–64.
- Tachibana K, Tachibana S. The use of ultrasound for drug delivery [review]. *Echocardiography* 2001;18:323–8.
- Kojima T, Mwale F, Yasuda T, Girard C, Poole AR, Laverty S. Early degradation of type IX and type II collagen with the onset of experimental inflammatory arthritis. *Arthritis Rheum* 2001;44:120–7.
- Sanchez-Pernaute O, Lopez-Armada MJ, Hernandez P, Palacios I, Navarro F, Martinez J, et al. Antifibroproliferative effect of tenidap in chronic antigen-induced arthritis. *Arthritis Rheum* 1997;40:2147–56.
- Gibson UE, Heid CA, Williams PM. A novel method for real time quantitative RT-PCR. *Genome Res* 1996;6:995–1001.
- Ward M, Wu J, Chiu JF. Experimental study of the effects of Optison concentration on sonoporation in vitro. *Ultrasound Med Biol* 2000;26:1169–75.
- Hui SW. The application of electroporation to transfect hematopoietic cells and to deliver drugs and vaccines transcutaneously for cancer treatment [review]. *Technol Cancer Res Treat* 2002;1:373–84.
- Lin YC, Li M, Wu CC. Simulation and experimental demonstration of the electric field assisted electroporation microchip for in vitro gene delivery enhancement. *Lab Chip* 2004;4:104–8.
- Weiss JM, Shivakumar R, Feller S, Li LH, Hanson A, Fogler WE, et al. Rapid, in vivo, evaluation of antiangiogenic and antineoplastic gene products by nonviral transfection of tumor cells. *Cancer Gene Ther* 2004;11:346–53.
- Shimizu T, Nikaido T, Gomyo H, Yoshimura Y, Horiuchi A, Isobe K, et al. Electrochemotherapy for digital chondrosarcoma. *J Orthop Sci* 2003;8:248–51.
- Abbing A, Blaschke UK, Grein S, Kretschmar M, Stark CM, Thies MJ, et al. Efficient intracellular delivery of a protein and a low molecular weight substance via recombinant polyomavirus-like particles. *J Biol Chem* 2004;279:27410–21.
- Ochi T, Iwase R, Kimura T, Hirooka A, Masada K, Owaki II, et al. Effect of early synovectomy on the course of rheumatoid arthritis. *J Rheumatol* 1991;18:1794–8.
- Hayem G, Domarle O, Thuong-Guyot M, Pocard JJ, Meyer O. Effects of methotrexate on the oxidative metabolism of cultured rabbit articular chondrocytes. *J Rheumatol* 2000;27:1117–20.
- Neidel J, Sova L, Schroers B, Sintermann F, Manzke O, Bohlen H. It is effects of methotrexate on normal articular cartilage in vitro and in vivo. *Ann Rheum Dis* 1998;57:414–21.
- Zhang ZJ, Huckle J, Francomano CA, Spencer RG. The effects of pulsed low-intensity ultrasound on chondrocyte viability, proliferation, gene expression and matrix production. *Ultrasound Med Biol* 2003;29:1645–51.
- Zhang ZJ, Huckle J, Francomano CA, Spencer RG. The influence of pulsed low-intensity ultrasound on matrix production of chondrocytes at different stages of differentiation: an explant study [published erratum appears in *Ultrasound Med Biol* 2003;29:1223]. *Ultrasound Med Biol* 2002;28:1547–53.
- Li T, Tachibana K, Kuroki M, Kuroki M. Gene transfer with echo-enhanced contrast agents: comparison between Alunex, Optison, and Levovist in mice: initial results. *Radiology* 2003;229:423–8.



Adiponectin increases bone mass by suppressing osteoclast and activating osteoblast

Kazuya Oshima^{a,b,1}, Akihide Nampei^{b,1}, Morihiko Matsuda^a, Masanori Iwaki^a,
Atsunori Fukuhara^a, Jun Hashimoto^b, Hideki Yoshikawa^b, Iichiro Shimomura^{a,c,d,*}

^a Department of Medicine and Pathophysiology, Graduate School of Frontier Biosciences, Osaka University, 2-2 Yamadaoka, Suita, Osaka 565-0871, Japan

^b Department of Orthopaedics, Graduate School of Medicine, Osaka University, 2-2 Yamadaoka, Suita, Osaka 565-0871, Japan

^c Department of Internal Medicine and Molecular Science, Graduate School of Medicine, Osaka University, 2-2 Yamadaoka, Suita, Osaka 565-0871, Japan

^d PRESTO, Japan Science and Technology Corporation (JST), 4-1-8 Honcho, Kawaguchi, Saitama 332-0012, Japan

Received 28 March 2005

Available online 8 April 2005

Abstract

Adiponectin, an adipose-derived hormone, exhibits various biological functions, such as increasing insulin sensitivity, protecting hypertension, and suppression of atherosclerosis, liver fibrosis, and tumor growth. Here, we report the role of adiponectin on bone metabolism. C57BL/6J mice were treated with adenovirus expressing lacZ or adiponectin, and their bones were analyzed by three-dimensional microcomputed tomography. Adiponectin-adenovirus treatment increased trabecular bone mass, accompanied by decreased number of osteoclasts and levels of plasma NTx, a bone-resorption marker. In vitro studies showed that adiponectin inhibited M-CSF- and RANKL-induced differentiation of mouse bone marrow macrophages and human CD14-positive mononuclear cells into osteoclasts and also suppressed the bone-resorption activity of osteoclasts. Furthermore, adiponectin enhanced mRNA expression of alkaline phosphatase and mineralization activity of MC3T3-E1 osteoblasts. Our results indicate that adiponectin exerts an activity to increase bone mass by suppressing osteoclastogenesis and by activating osteoblastogenesis, suggesting that adiponectin manipulation could be therapeutically beneficial for patients with osteopenia.

© 2005 Elsevier Inc. All rights reserved.

Keywords: Bone mass; Adiponectin; Adipose tissue; Adipocytokines; Osteoclasts; Osteoblasts; Bone metabolism; Osteopenia

Osteoporosis and related bone fractures are growing medical problems especially with the enhanced longevity in industrial countries [1,2]. Therefore, it is important to know the factors that regulate bone mass and to develop effective therapeutic methods. Bone and bone marrow consist of various cells, including osteoblasts, osteoclasts, hematopoietic cells, and adipocytes. Bone adipocytes share a common mesenchymal precursor with

osteoblasts and chondrocytes, and their numbers in bone marrow are altered in various pathophysiological conditions [3,4], but their roles in bone biology have not been clarified.

Several studies of adipocyte function have revealed that adipose tissue is not merely an energy-storing organ but it secretes a variety of biologically active molecules, which we conceptualized as “adipocytokines,” including plasminogen activator inhibitor-1, tumor necrosis factor- α , resistin, leptin, and adiponectin [5–8]. Recent studies suggested that leptin, an anti-satiety adipocytokine, might have enhancing effects on bone mass

* Corresponding author. Fax: +81 6 6879 3739.

E-mail address: ichi@imed2.med.osaka-u.ac.jp (I. Shimomura).

¹ These two authors contributed equally to this work.

[9,10]. Administration of leptin partially prevented bone loss in ovariectomized rats [11] and increased bone mineral density in leptin-deficient mice [12,13].

Adiponectin is a fat-specific secretory factor that was identified by our group in human fat cDNA [14]. The mouse homologue of adiponectin was independently cloned as adipoQ and Acrp30 [15,16]. We and others have shown that adiponectin has various biological functions, such as increasing insulin sensitivity in the liver and skeletal muscle, and protecting vascular walls from atherosclerosis, hence low plasma adiponectin levels in obesity might contribute to insulin resistance, diabetes, and atherosclerosis [17–21]. Furthermore, we recently showed that adiponectin inhibited liver fibrosis by suppressing proliferation and activity of hepatic stellate cells producing fibrotic collagen and transforming growth factor- β [22]. Others also reported that adiponectin have tumor growth inhibitory properties [23]. On the other hand, receptors of adiponectin were cloned and found to be expressed ubiquitously [24–26], suggesting that adiponectin might also play certain roles in bone biology.

The present study was designed to determine the effects of adiponectin on bone metabolism. The results showed that adiponectin increased bone mass by suppressing osteoclastogenesis and by activating osteoblastogenesis, suggesting that adiponectin could be potentially useful therapeutically for patients with reduced bone mass.

Materials and methods

Animals. All animals were purchased from Clea Japan (Tokyo, Japan) and housed in a room under controlled temperature ($23 \pm 1^\circ\text{C}$) and humidity (45–65%), and had free access to water and chow (Oriental Yeast). All animal experiments were conducted in accordance with the Institutional Guidelines for the Care and Use of laboratory animals.

Adiponectin adenovirus. Adenovirus producing the full-length mouse adiponectin was prepared as described previously [27]. Then, 2×10^8 plaque-forming units of adenovirus-adiponectin (Ad-adipo) or adenovirus-lacZ (Ad-lacZ) were injected into the jugular vein of 8-week-old C57BL/6J male mice. Mice were sacrificed on day 14 after virus injection.

Skeletal morphology. Three-dimensional microcomputed tomography (3D- μCT) scan was undertaken and the trabecular bone area (percentage of bone volume [BV] per tissue volume [TV]) was measured using a composite X-ray analysis system (Shimadzu, SMX-100CT-SV, Kyoto, Japan). Bones were fixed in 10% buffered formalin, decalcified in 14% ethylenediaminetetraacetic acid (EDTA), and embedded in paraffin. The sections were stained with tartrate-resistant acid phosphate (TRAP) and the number of TRAP-positive cells was counted in five sections per mouse.

Bone marker measurement. The blood samples were collected on day 14 after virus injection and processed within 30 min of collection, and aliquots of plasma were kept frozen at -80°C until analyzed. Plasma cross-linked N-telopeptide of type I collagen (NTx), which is a marker of bone resorption, was measured by using an enzyme immunoassay (EIA). NTx concentrations were expressed as nanomoles of bone collagen equivalents (BCE) per liter (nM BCE/L).

Culture of mouse bone marrow macrophages. Mouse bone marrow macrophages (M-BMMs) were obtained as reported previously [28].

Briefly, whole bone marrow cells prepared from the femur and tibia of 5-week-old C57BL/6J male mice were suspended in α -minimal essential medium (α MEM) containing 10% heat-inactivated fetal bovine serum (FBS) and recombinant human macrophage colony-stimulating factor (M-CSF, 100 ng/ml) at 5×10^6 cells in a 10-cm culture dish. After 3 days in culture, the cells were washed, harvested with 0.02% EDTA in phosphate-buffered saline (PBS), and seeded at 3×10^5 cells into another 10-cm culture dish. After a further 3 days in culture, the cells were harvested, plated at a density of 1.5×10^4 cells/cm² in 48-well plates, and maintained for 5 days in the presence of recombinant human soluble receptor activator of nuclear factor- κ B ligand (RANKL, 50 ng/ml) and M-CSF (100 ng/ml) with or without recombinant human adiponectin [29].

Culture of human CD14⁺ peripheral blood mononuclear cells. Human CD14-positive peripheral blood mononuclear cells (PBMCs) were prepared as reported previously [30]. Briefly, peripheral blood was obtained from healthy male volunteers and was carefully layered on the Ficoll-Paque PLUS solution (Amersham Biosciences, USA), and centrifuged at 1500 rpm for 30 min. PBMC layer was collected and washed twice in PBS. CD14-positive cells were selected using a magnetic isolation procedure (MACS CD14 Microbeads, Miltenyi Biotec, Germany). The cells were plated at a density of 1×10^5 cells/cm² in 48-well plates in α MEM containing 10% FBS and 1% penicillin/streptomycin, and cultured for 7 days in the presence of M-CSF (25 ng/ml) and RANKL (40 ng/ml) with or without recombinant human adiponectin.

Tartrate-resistant acid phosphate staining. TRAP staining was performed using a commercial TRAP staining kit (Hokudo, Sapporo, Japan). The number of TRAP-positive multinuclear (>3 nuclei) cells in each well was counted.

Calcium resorption assay. Calcified matrix-resorption activity of osteoclasts was determined using BD BioCoat osteologic calcium hydroxyapatite-coated 16-well chamber slides (BD Biosciences, Bedford, MA). Human CD14-positive monocytes were seeded at a density of 1×10^5 cells/cm² with M-CSF (25 ng/ml) and RANKL (40 ng/ml). At day 0, 3 (pre-osteoclasts) or day 7 (mature osteoclasts), recombinant human adiponectin was added to the culture medium. At day 14 cells were removed by vigorous washing, and resorption area was measured using Win Roof software version 3.5 (Mitani, Fukui, Japan).

Cell culture. Mouse pre-osteoblast MC3T3-E1 cells were cultured in α MEM supplemented with 10% FBS and 1% penicillin/streptomycin. For cell differentiation study, the cells were seeded at a density of 2×10^4 per well in 12-well plates. After the cultures reached confluence, the medium was changed to α MEM with 10% FBS containing 50 $\mu\text{g/ml}$ L-ascorbic acid phosphate magnesium (Wako Pure Chemical, Osaka, Japan) and 10 mM β -glycerophosphate (Wako Pure Chemical). Then, the cells were further cultured for indicated time with or without recombinant mouse adiponectin, which was generated in a manner similar to recombinant human adiponectin as described previously [31].

RNA analysis. Total RNAs were extracted from cells with an RNA-STAT-60 kit (Tel-Test "B"). The first-strand cDNA was synthesized using ThermoScript RT-PCR System (Invitrogen, San Diego, CA). Real-time polymerase chain reaction (PCR) was performed on a Light Cycler using the Fast Start DNA Master SYBR Green I (Roche Diagnostics) according to the protocol provided by the manufacturer [32]. Sequences of primers used for real-time PCR were as follows: alkaline phosphatase (ALP), 5'-GCC CTC TCC AAG ACA TAT A-3' and 5'-CCA TGA TCA CGT CGA TAT CC-3', 18S, 5'-CGG CTA CCA CAT CCA AGG AA-3' and 5'-GCT GGA ATT ACC GCG GCT-3'.

Mineralization assay. MC3T3-E1 cells were incubated at 34°C for 24 h in culture medium, and then the medium was refreshed with culture medium with or without adiponectin. The degree of mineralization was determined in the 12-well plates using Alizarin Red staining, as described previously [33]. Briefly, the differentiated MC3T3-E1 cells were rinsed twice with PBS followed by fixation with 70% ethanol for 1 h at room temperature. Then cells were stained with 40 mM

Alizarin Red S (Wako Pure Chemical) at pH 4.0 for 10 min at room temperature, and were washed five times with deionized water and twice with PBS. Then, staining was released from the cell matrix by incubation in 10% cetylpyridinium chloride at pH 7.0 for 15 min. The degree of mineralization was determined by measuring the absorbance of supernatants at 562 nm.

Statistical analysis and ethical considerations. Results were expressed as means \pm SEM. Differences between groups were examined for statistical significance using Student's *t* test or analysis of variance with Fisher's protected least significant difference test. A *P* value less than 0.05 denoted the presence of a statistically significant difference. The experimental protocol was approved by the Ethics Review Committee for Animal Experimentation of Osaka University School of Medicine.

Results

Adenovirus-mediated overexpression of adiponectin in vivo

To investigate the in vivo role of adiponectin in bone metabolism, we treated C57BL/6J mice with adenovirus producing adiponectin (Ad-adipo) or lacZ (Ad-lacZ). Two weeks after injection, we estimated structural changes in the bone by analyzing cortical and trabecular bones with 3D- μ CT. Fig. 1A shows representative 3D- μ CT images of the proximal tibia of Ad-lacZ- and Ad-adipo-treated mice, demonstrating a significantly larger trabecular bone volume in Ad-adipo-treated mice than in Ad-lacZ-treated mice. The trabecular bone volume of the proximal tibia at two different areas located 50–250 and 500–700 μ m from the growth plates of the proximal tibia (representing the most active areas for bone remodeling, Fig. 1B) was significantly higher in Ad-adipo-treated mice than in the control Ad-lacZ-treated mice (Fig. 1B). Similar findings were observed in the femur, by 3D- μ CT analysis (data not shown).

To investigate whether adiponectin modulates osteoclastogenesis, we analyzed TRAP-stained sections of the distal femur in Ad-lacZ- and Ad-adipo-treated mice. Examination of these sections demonstrated fewer TRAP-positive osteoclasts in Ad-adipo-treated mice than in Ad-lacZ-treated mice (Fig. 2A). Quantitative analysis confirmed that the number of TRAP-positive osteoclasts was significantly lower in adiponectin-adenovirus-treated mice than in Ad-lacZ-treated mice (Fig. 2B). Furthermore, in Ad-adipo-treated mice, plasma levels of NTx, a marker of bone resorption, were significantly lower than in Ad-lacZ-treated mice (Fig. 2C). Taken together, our in vivo data indicated that adiponectin suppresses osteoclastogenesis.

Effects of adiponectin on osteoclast differentiation and activity

Next, we investigated the effects of adiponectin on the differentiation of osteoclasts in vitro by treating primary cultures of bone marrow stromal cells, which contain

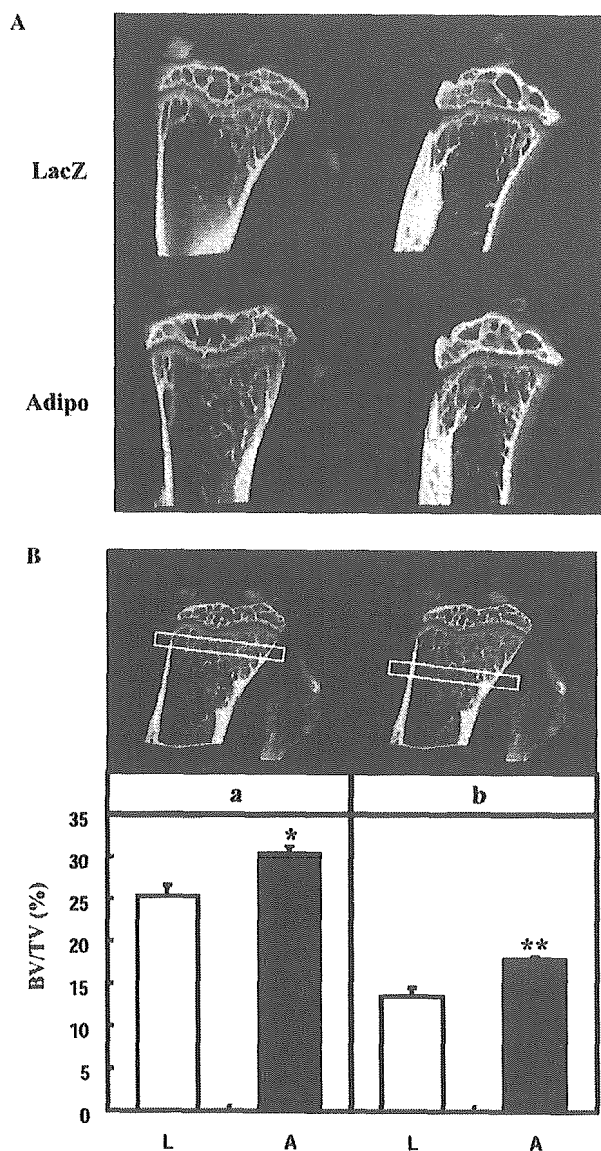


Fig. 1. Increased trabecular bone mass in adiponectin-adenovirus-treated mice. (A) Three-dimensional μ CT scan images of the proximal tibia of C57BL/6J mice treated with lacZ- (upper panels) or adiponectin-adenovirus (lower panels). The left-side panels show anterior–posterior view and the right-side panels show lateral–medial view. (B) Quantitative data of trabecular bone volume at indicated two areas; 50–250 μ m (a) and 500–700 μ m (b) from the distal end of the growth plate, in the proximal tibia of C57BL/6J mice treated with lacZ- (L, $n = 8$) and adiponectin-adenovirus (A, $n = 8$). Data are expressed as percentage of total tissue volume (BV/TV [%]). Data are means \pm SEM. * $P < 0.05$, ** $P < 0.01$, compared with lacZ-adenovirus-treated mice.

osteoclast progenitor cells, with or without recombinant adiponectin. Previous studies reported that M-CSF and RANKL induced differentiation of progenitor cells into TRAP-positive osteoclasts [34,35]. In the present study, treatment of bone marrow stromal cells with adiponectin suppressed M-CSF/RANKL-induced differentiation of these cells into osteoclasts, in a dose-dependent

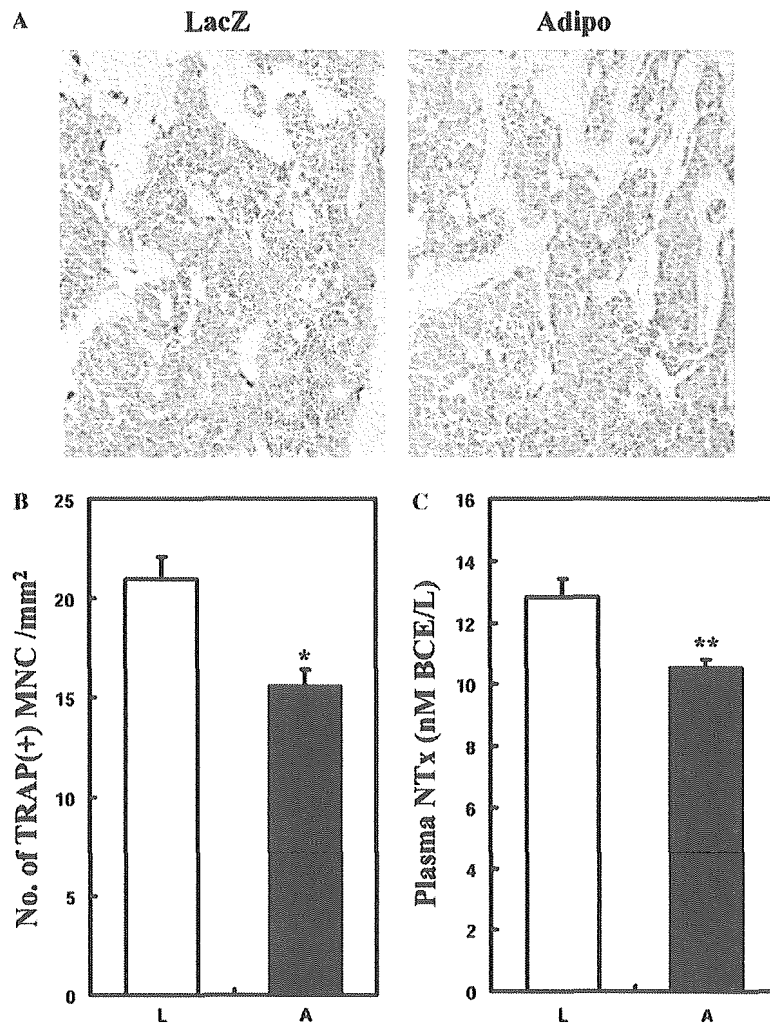


Fig. 2. Reduction of TRAP-positive osteoclasts in mice treated with adiponectin-adenovirus. (A) Histological examination of the distal femur with TRAP staining (left; lacZ, right; adiponectin). TRAP-positive osteoclasts are stained red. (B) Quantitative analysis of the number of TRAP-positive osteoclasts in C57BL/6J mice treated with lacZ- (L, $n = 8$) and adiponectin-adenovirus (A, $n = 8$). Data are means \pm SEM. * $P < 0.05$, compared with lacZ-adenovirus-treated mice. (C) Plasma NTx levels of C57BL/6J mice treated with lacZ- (L, $n = 8$) and adiponectin-adenovirus (A, $n = 8$). Data are means \pm SEM. ** $P < 0.01$, compared with lacZ-adenovirus-treated mice. (For interpretation of the references to color in this figure legend, the reader is referred to the web version of this paper.)

manner (Fig. 3A). Similarly, adiponectin also dose-dependently suppressed differentiation of human CD14-positive PBMCs into osteoclasts (Fig. 3B).

Next, we performed bone-resorption analyses with or without adiponectin treatment, using human CD14-positive cells. Treatment of these cells with adiponectin for 14 days (days 0–14) after M-CSF- and RANKL-induced differentiation resulted in a significant reduction of the resorption area in a dose-dependent manner (Fig. 3C). Furthermore, a significant reduction of the resorption area was also noted with adiponectin treatment from day 3 or 7 when human CD14-positive cells were already differentiated (days 3–14, 7–14) (Figs. 3D and E). These results suggest that adiponectin could suppress osteoclastogenesis and bone-resorption activity of osteoclasts.

Effects of adiponectin on MC3T3-E1 osteoblasts

To investigate the effects of adiponectin on osteoblasts, we treated MC3T3-E1 osteoblasts with adiponectin for 18 days and measured mRNA levels of alkaline phosphatase (ALP) and the mineralization activity of MC3T3-E1 osteoblasts. Treatment with adiponectin significantly increased ALP mRNA level on day 12 and 18 compared with the control (Fig. 4A), suggesting that adiponectin might enhance the differentiation of osteoblasts. Previous reports indicated increased mineralization activity of MC3T3-E1 cell matrix in the presence of ascorbic acid [33,36]. Treatment of these cells with adiponectin significantly increased mineralization of the matrix (Fig. 4B).

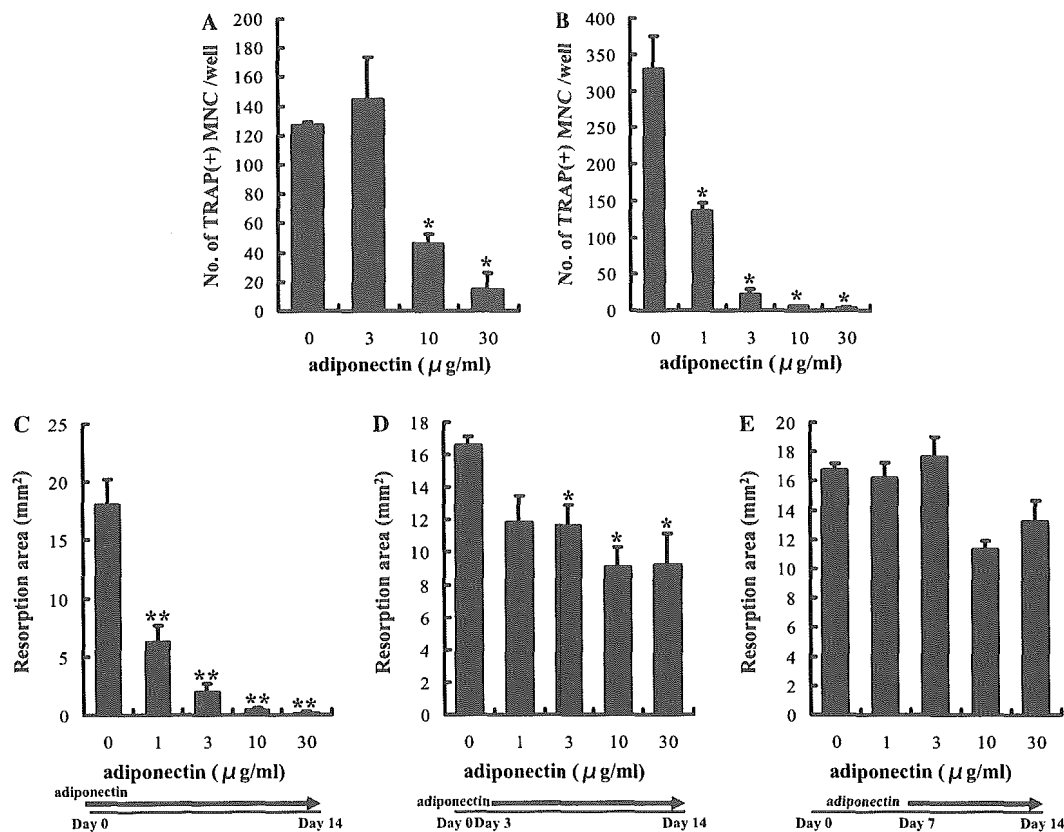


Fig. 3. Effects of adiponectin on primary cultures of osteoclasts. (A,B) TRAP assay of primary cultures of mouse bone marrow macrophages (A) and human CD14-positive PBMCs (B) stimulated by M-CSF and RANKL and treated with the indicated amounts of adiponectin. Data are expressed as means \pm SEM. * P < 0.05, compared with cells that were not treated with adiponectin (0–30 μ g/ml). (C, D, and E) Bone-resorption assay of human CD14-positive PBMCs stimulated by M-CSF and RANKL, and treated with the indicated amounts of adiponectin from day 0 to 14 (C), from day 3 to 14 (D), and from day 7 to 14 (E). Data are means \pm SEM. * P < 0.05, ** P < 0.01, compared with cells that were not treated with adiponectin (0–30 μ g/ml).

Discussion

In the present study, we investigated the role of adiponectin on bone formation *in vivo*, using an adiponectin-producing adenovirus. The major finding of the present study was that adiponectin supplement increased bone mass in trabecular bone. Analysis of the mechanism of this action revealed that adiponectin acts by reducing the differentiation and bone-resorption activity of osteoclasts, and possibly by enhancing the differentiation and mineralization activity of osteoblasts.

We observed the increase of bone mass only in trabecular bone, but not in cortical bone, of adiponectin-adenovirus-treated mice. The duration of adiponectin overproduction by adenovirus treatment is at most 2 weeks. This could explain, at least in part, the effect of adiponectin on trabecular bone and the lack of such effect on cortical bone, since the former has a higher remodeling activity than the latter [37]. We also observed a significant decrease in osteoclast count and plasma NTx levels in adiponectin-adenovirus-treated

mice, indicating that adiponectin inhibits bone resorption. These findings were confirmed in tissue culture experiments. In mouse bone marrow macrophages (M-BMMs) and CD14-positive human peripheral blood mononuclear cells (PBMCs), adiponectin inhibited the M-CSF- and RANKL-induced differentiation of these cells into osteoclasts, as well as the bone-resorption activity of mature osteoclasts. Furthermore, we found that both bone tissue and primary osteoclasts expressed both adiponectin receptors (AdipoR1 and R2) (Supplemental Fig. 1), suggesting that adiponectin directly targets osteoclast cells. These results demonstrate that adiponectin suppresses bone-resorption activity by inhibiting osteoclastogenesis.

In adiponectin-adenovirus infected mice, plasma glucose and insulin levels did not change compared to control-adenovirus infected mice, indicating that this adenovirus treatment did not affect glucose metabolism systemically (data not shown). This is consistent with our previous report, in which we demonstrated that adiponectin-KO mice showed normal glucose and insulin levels in plasma, and adiponectin-adenovirus has no

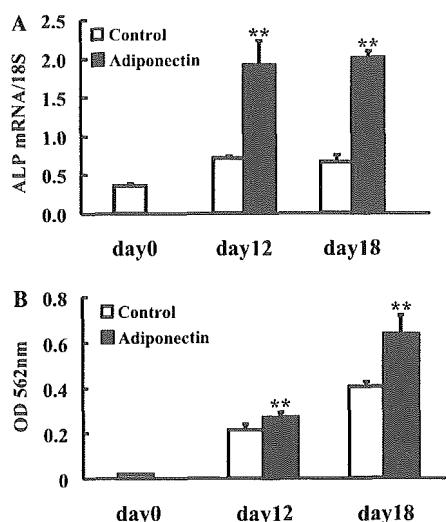


Fig. 4. Effects of adiponectin on MC3T3-E1 osteoblasts. (A) ALP mRNAs in MC3T3-E1 cells treated with or without adiponectin for 12 or 18 days were measured by real-time quantitative reverse transcriptase-PCR as described in Materials and methods. Data are normalized with 18S RNAs and expressed as means \pm SEM of three independent experiments. $**P < 0.01$, compared with the control. (B) The mineralization activity of MC3T3-E1 cells treated with or without adiponectin for 12 or 18 days was measured as described in Materials and methods. Data are expressed as means \pm SEM of three independent experiments. $**P < 0.01$, compared with the control.

effect on plasma glucose and insulin levels under control diet, although when adiponectin-KO mice are fed with high fat diet, their plasma glucose and insulin levels significantly elevate compared to wild-type mice and adiponectin-adenovirus reverses them to the level of wild-type mice [19]. Therefore, this effect of adiponectin should not be mediated by its systemic insulin-sensitizing effect in normal mice. However, whether it is mediated by local insulin-sensitizing effect remains to be elucidated.

The bone-forming activity of osteoblasts is also important in determining bone mass [37,38]. Our study revealed that adiponectin increased mRNA expression of ALP and mineralization activity of mouse MC3T3-E1 osteoblasts. We also investigated the effect of adiponectin on the osteoblastogenesis of primary mouse osteoblasts and mouse bone marrow cells. However, the effect was not significant on these cells (data not shown), indicating that adiponectin may have the potential to activate osteoblasts, but its effect may be dependent on the cell types.

In conclusion, we have demonstrated in the present study that adiponectin increases bone mass by suppressing osteoclastogenesis and possibly by activating osteoblastogenesis. These results suggest that increasing the concentration and/or enhancing the activity of adiponectin might be therapeutically beneficial for patients with reduced bone mass.

Acknowledgments

We are grateful to F. Ikeda, R. Nishimura, T. Yoneda, and K. Sudo for the excellent technical assistance. We thank all members of Shimomura's laboratory for the helpful discussion and comments. This study was supported in part by Yamanouchi Pharmaceutical Co., Ltd., Suzuken Memorial Foundation, The Tokyo Biochemical Research Foundation, Takeda Medical Research Foundation, Uehara Memorial Foundation, Takeda Science Foundation, Novartis Foundation (Japan) for the Promotion of Science, The Cell Science Research Foundation, The Mochida Memorial Foundation for Medical and Pharmaceutical Research, Grant-in-Aid from the Japan Medical Association, The Naito Foundation, a grant from the Japan Heart Foundation Research, Kato Memorial Bioscience Foundation, Japan Research Foundation for Clinical Pharmacology, The 21st Century COE Program, Japan, grants from the Ministry of Health, Labour and Welfare, Japan, and grants from the Ministry of Education, Culture, Sports, Science and Technology, Japan.

Appendix A. Supplementary data

Supplementary data associated with this article can be found, in the online version, at doi:10.1016/j.bbrc.2005.03.210.

References

- [1] D.M. Smith, M.R. Khairi, C.C. Johnston Jr., The loss of bone mineral with aging and its relationship to risk of fracture, *J. Clin. Invest.* 56 (1975) 311–318.
- [2] B.L. Riggs, L.J. Melton, Involutional osteoporosis, *N. Engl. J. Med.* 314 (1986) 1676–1686.
- [3] M.F. Pittenger, A.M. Mackay, S.C. Beck, R.K. Jaiswal, R. Douglas, J.D. Mosca, M.A. Moorman, D.W. Simonetti, S. Craig, D.R. Marshak, Multilineage potential of adult human mesenchymal stem cells, *Science* 284 (1999) 143–147.
- [4] J.E. Dennis, A. Merriam, A. Awadallah, J.U. Yoo, B. Johnstone, A.I. Caplan, A quadripotential mesenchymal progenitor cell isolated from the marrow of an adult mouse, *J. Bone Miner. Res.* 14 (1999) 700–709.
- [5] I. Shimomura, T. Funahashi, M. Takahashi, K. Maeda, K. Kotani, T. Nakamura, S. Yamashita, M. Miura, Y. Fukuda, K. Takemura, K. Tokunaga, Y. Matsuzawa, Enhanced expression of PAI-1 in visceral fat: possible contributor to vascular disease in obesity, *Nat. Med.* 2 (1996) 800–803.
- [6] G.S. Hotamisligil, N.S. Shargill, B.M. Spiegelman, Adipose expression of tumor necrosis factor- α : direct role in obesity-linked insulin resistance, *Science* 259 (1993) 87–91.
- [7] C.M. Steppan, S.T. Bailey, S. Bhat, E.J. Brown, R.R. Banerjee, C.M. Wright, H.R. Patel, R.S. Ahima, M.A. Lazar, The hormone resistin links obesity to diabetes, *Nature* 409 (2001) 307–312.
- [8] J.M. Friedman, J.L. Halaas, Leptin and the regulation of body weight in mammals, *Nature* 395 (1998) 763–770.
- [9] P. Laharrague, D. Larrouy, A.M. Fontanilles, N. Truel, A. Campfield, R. Tenenbaum, J. Galitzky, J.X. Corberand,

- L. Penicaud, L. Casteilla, High expression of leptin by human bone marrow adipocytes in primary culture, *FASEB J.* 12 (1998) 747–752.
- [10] T. Thomas, F. Gori, S. Khosla, M.D. Jensen, B. Burguera, B.L. Riggs, Leptin acts on human marrow stromal cells to enhance differentiation to osteoblasts and to inhibit differentiation to adipocytes, *Endocrinology* 140 (1999) 1630–1638.
- [11] B. Burguera, L.C. Hofbauer, T. Thomas, F. Gori, G.L. Evans, S. Khosla, B.L. Riggs, R.T. Turner, Leptin reduces ovariectomy-induced bone loss in rats, *Endocrinology* 142 (2001) 3546–3553.
- [12] C.M. Steppan, D.T. Crawford, K.L. Chidsey-Frink, H. Ke, A.G. Swick, Leptin is a potent stimulator of bone growth in ob/ob mice, *Regul. Pept.* 92 (2000) 73–78.
- [13] P. Ducy, M. Amling, S. Takeda, M. Priemel, A.F. Schilling, F.T. Beil, J. Shen, C. Vinson, J.M. Rueger, G. Karsenty, Leptin inhibits bone formation through a hypothalamic relay: a central control of bone mass, *Cell* 100 (2000) 197–207.
- [14] K. Maeda, K. Okubo, I. Shimomura, T. Funahashi, Y. Matsuzawa, K. Matsubara, cDNA cloning and expression of a novel adipose specific collagen-like factor, apM1 (AdiPose Most abundant Gene transcript 1), *Biochem. Biophys. Res. Commun.* 221 (1996) 286–289.
- [15] P.E. Scherer, S. Williams, M. Fogliano, G. Baldini, H.F. Lodish, A novel serum protein similar to C1q, produced exclusively in adipocytes, *J. Biol. Chem.* 270 (1995) 26746–26749.
- [16] E. Hu, P. Liang, B.M. Spiegelman, AdipoQ is a novel adipose-specific gene dysregulated in obesity, *J. Biol. Chem.* 271 (1996) 10697–10703.
- [17] T. Yamauchi, J. Kamon, H. Waki, Y. Terauchi, N. Kubota, K. Hara, Y. Mori, T. Ide, K. Murakami, N. Tsuboyama-Kasaoka, O. Ezaki, Y. Akanuma, O. Gavrilova, C. Vinson, M.L. Reitman, H. Kagechika, K. Shudo, M. Yoda, Y. Nakano, K. Tobe, R. Nagai, S. Kimura, M. Tomita, P. Froguel, T. Kadowaki, The fat-derived hormone adiponectin reverses insulin resistance associated with both lipotrophy and obesity, *Nat. Med.* 7 (2001) 941–946.
- [18] A.H. Berg, T.P. Combs, X. Du, M. Brownlee, P.E. Scherer, The adipocyte-secreted protein Acrp30 enhances hepatic insulin action, *Nat. Med.* 7 (2001) 947–953.
- [19] N. Maeda, I. Shimomura, K. Kishida, H. Nishizawa, M. Matsuda, H. Nagaretani, N. Furuyama, H. Kondo, M. Takahashi, Y. Arita, R. Komuro, N. Ouchi, S. Kihara, Y. Tochino, K. Okutomi, M. Horie, S. Takeda, T. Aoyama, T. Funahashi, Y. Matsuzawa, Diet-induced insulin resistance in mice lacking adiponectin/ACRP30, *Nat. Med.* 8 (2002) 731–737.
- [20] T. Yamauchi, J. Kamon, Y. Minokoshi, Y. Ito, H. Waki, S. Uchida, S. Yamashita, M. Noda, S. Kita, K. Ueki, K. Eto, Y. Akanuma, P. Froguel, F. Foufelle, P. Ferre, D. Carling, S. Kimura, R. Nagai, B.B. Kahn, T. Kadowaki, Adiponectin stimulates glucose utilization and fatty-acid oxidation by activating AMP-activated protein kinase, *Nat. Med.* 8 (2002) 1288–1295.
- [21] P.A. Jansson, F. Pellme, A. Hammarstedt, M. Sandqvist, H. Brekke, K. Caidahl, M. Forsberg, R. Volkman, E. Carvalho, T. Funahashi, Y. Matsuzawa, O. Wiklund, X. Yang, M.R. Taskinen, U. Smith, A novel cellular marker of insulin resistance and early atherosclerosis in humans is related to impaired fat cell differentiation and low adiponectin, *FASEB J.* 17 (2003) 1434–1440.
- [22] Y. Kamada, S. Tamura, S. Kiso, H. Matsumoto, Y. Saji, Y. Yoshida, K. Fukui, N. Maeda, H. Nishizawa, H. Nagaretani, Y. Okamoto, S. Kihara, J. Miyagawa, Y. Shinomura, T. Funahashi, Y. Matsuzawa, Enhanced carbon tetrachloride-induced liver fibrosis in mice lacking adiponectin, *Gastroenterology* 125 (2003) 1796–1807.
- [23] E. Brakenhielm, N. Veitonmaki, R. Cao, S. Kihara, Y. Matsuzawa, B. Zhiyotovskiy, T. Funahashi, Y. Cao, Adiponectin-induced antiangiogenesis and antitumor activity involve caspase-mediated endothelial cell apoptosis, *Proc. Natl. Acad. Sci. USA* 101 (2004) 2476–2481.
- [24] T. Yamauchi, J. Kamon, Y. Ito, A. Tsuchida, T. Yokomizo, S. Kita, T. Sugiyama, M. Miyagishi, K. Hara, M. Tsunoda, K. Murakami, T. Ohteki, S. Uchida, S. Takekawa, N. Waki, N.H. Tsuno, Y. Shibata, Y. Terauchi, P. Froguel, K. Tobe, S. Koyasu, K. Taira, T. Kitamura, T. Shimizu, R. Nagai, T. Kadowaki, Cloning of adiponectin receptors that mediate antidiabetic metabolic effects, *Nature* 423 (2003) 762–769.
- [25] H. Staiger, S. Kaltenbach, K. Staiger, N. Stefan, A. Fritsche, A. Guirguis, C. Peterfi, M. Weisser, F. Machicao, M. Stumvoll, H.U. Haring, Expression of adiponectin receptor mRNA in human skeletal muscle cells is related to in vivo parameters of glucose and lipid metabolism, *Diabetes* 53 (2004) 2195–2201.
- [26] G. Chinetti, C. Zawadzki, J.C. Fruchart, B. Staels, Expression of adiponectin receptors in human macrophages and regulation by agonists of the nuclear receptors PPARalpha, PPARgamma, and LXR, *Biochem. Biophys. Res. Commun.* 314 (2004) 151–158.
- [27] M. Matsuda, I. Shimomura, M. Sata, Y. Arita, M. Nishida, N. Maeda, M. Kumada, Y. Okamoto, H. Nagaretani, H. Nishizawa, K. Kishida, R. Komuro, N. Ouchi, S. Kihara, R. Nagai, T. Funahashi, Y. Matsuzawa, Role of adiponectin in preventing vascular stenosis. The missing link of adipo-vascular axis, *J. Biol. Chem.* 277 (2002) 37487–37491.
- [28] Y. Azuma, K. Kaji, R. Katogi, S. Takeshita, A. Kudo, Tumor necrosis factor-alpha induces differentiation of and bone resorption by osteoclasts, *J. Biol. Chem.* 275 (2000) 4858–4864.
- [29] H. Yasuda, N. Shima, N. Nakagawa, K. Yamaguchi, M. Kinoshita, S. Mochizuki, A. Tomoyasu, K. Yano, M. Goto, A. Murakami, E. Tsuda, T. Morinaga, K. Higashio, N. Udagawa, N. Takahashi, T. Suda, Osteoclast differentiation factor is a ligand for osteoprotegerin/osteoclastogenesis-inhibitory factor and is identical to TRANCE/RANKL, *Proc. Natl. Acad. Sci. USA* 95 (1998) 3597–3602.
- [30] G.C. Nicholson, M. Malakellis, F.M. Collier, P.U. Cameron, W.R. Holloway, T.J. Gough, C. Gregorio-King, M.A. Kirkland, D.E. Myers, Induction of osteoclasts from CD14-positive human peripheral blood mononuclear cells by receptor activator of nuclear factor kappaB ligand (RANKL), *Clin. Sci. Lond.* 99 (2000) 133–140.
- [31] Y. Arita, S. Kihara, N. Ouchi, M. Takahashi, K. Maeda, J. Miyagawa, K. Hotta, I. Shimomura, T. Nakamura, K. Miyaoka, H. Kuriyama, M. Nishida, S. Yamashita, K. Okubo, K. Matsubara, M. Muraguchi, Y. Ohmoto, T. Funahashi, Y. Matsuzawa, Paradoxical decrease of an adipose-specific protein, adiponectin, in obesity, *Biochem. Biophys. Res. Commun.* 257 (1999) 79–83.
- [32] M. Iwaki, M. Matsuda, N. Maeda, T. Funahashi, Y. Matsuzawa, M. Makishima, I. Shimomura, Induction of adiponectin, a fat-derived antidiabetic and antiatherogenic factor, by nuclear receptors, *Diabetes* 52 (2003) 1655–1663.
- [33] T. Maeda, A. Matsunuma, T. Kawane, N. Horiuchi, Simvastatin promotes osteoblast differentiation and mineralization in MC3T3-E1 cells, *Biochem. Biophys. Res. Commun.* 280 (2001) 874–877.
- [34] T. Tsurukai, N. Udagawa, K. Matsuzaki, N. Takahashi, T. Suda, Roles of macrophage-colony stimulating factor and osteoclast differentiation factor in osteoclastogenesis, *J. Bone Miner. Metab.* 18 (2000) 177–184.
- [35] S. Takeshita, K. Kaji, A. Kudo, Identification and characterization of the new osteoclast progenitor with macrophage phenotypes being able to differentiate into mature osteoclasts, *J. Bone Miner. Res.* 15 (2000) 1477–1488.
- [36] R.T. Franceschi, B.S. Iyer, Relationship between collagen synthesis and expression of the osteoblast phenotype in MC3T3-E1 cells, *J. Bone Miner. Res.* 7 (1992) 235–246.
- [37] J.A. Buckwalter, R.R. Cooper, Bone structure and function, *Instr. Course Lect.* 36 (1987) 27–48.
- [38] T. Katagiri, N. Takahashi, Regulatory mechanisms of osteoblast and osteoclast differentiation, *Oral Dis.* 8 (2002) 147–159.

A new biotechnology for articular cartilage repair: subchondral implantation of a composite of interconnected porous hydroxyapatite, synthetic polymer (PLA-PEG), and bone morphogenetic protein-2 (rhBMP-2)

Noriyuki Tamai M.D., Ph.D.†, Akira Myoui M.D., Ph.D.†, Makoto Hirao M.D.†, Takashi Kaito M.D.†, Takahiro Ochi M.D., Ph.D.†, Junzo Tanaka Ph.D.§, Kunio Takaoka M.D., Ph.D.|| and Hideki Yoshikawa M.D., Ph.D.†*

† Department of Orthopaedic Surgery, Osaka University Graduate School of Medicine, 2-2 Yamadaoka, Suita, Osaka 565-0871, Japan

‡ National Hospital Organization Sagamihara National Hospital, 18-1 Sakuradai, Sagamihara, Kanagawa 228-8522, Japan

§ Biomaterials Center, National Institute for Materials Science, 1-1 Namiki, Tsukuba, Ibaraki 305-0044, Japan

|| Department of Orthopaedic Surgery, Osaka City University Medical School, 1-4-3 Asahimachi, Abeno-ku, Osaka 545-8585, Japan

Summary

Objective: Articular cartilage repair remains a major obstacle in tissue engineering. We recently developed a novel tool for articular cartilage repair, consisting of a triple composite of an interconnected porous hydroxyapatite (IP-CHA), recombinant human bone morphogenetic protein-2 (rhBMP-2), and a synthetic biodegradable polymer [poly-D,L-lactic acid/polyethylene glycol (PLA-PEG)] as a carrier for rhBMP-2. In the present study, we evaluated the capacity of the triple composite to induce the regeneration of articular cartilage.

Methods: Full-thickness cartilage defects were created in the trochlear groove of 52 New Zealand White rabbits. Sixteen defects were filled with the bone morphogenetic protein (BMP)/PLA-PEG/IP-CHA composite (group I), 12 with PLA-PEG/IP-CHA (group II), 12 with IP-CHA alone (group III), and 12 were left empty (group IV). The animals were killed 1, 3, and 6 weeks after surgery, and the gross appearance of the defect sites was assessed. The harvested tissues were examined radiographically and histologically.

Results: One week after implantation with the BMP/PLA-PEG/IP-CHA composite (group I), vigorous repair had occurred in the subchondral defect. It contained an agglomeration of mesenchymal cells which had migrated from the surrounding bone marrow either directly, or indirectly via the interconnecting pores of the IP-CHA scaffold. At 6 weeks, these defects were completely repaired. The regenerated cartilage manifested a hyaline-like appearance, with a mature matrix and a columnar organization of chondrocytes.

Conclusions: The triple composite of rhBMP-2, PLA-PEG, and IP-CHA promotes the repair of full-thickness articular cartilage defects within as short a period as 3 weeks in the rabbit model. Hence, this novel cell-free implant biotechnology could mark a new development in the field of articular cartilage repair.

© 2005 OsteoArthritis Research Society International. Published by Elsevier Ltd. All rights reserved.

Key words: Articular cartilage repair, Interconnected porous hydroxyapatite (IP-CHA), BMP, PLA-PEG.

Introduction

To date, the myth “once destroyed, cartilage cannot be repaired” has yet to be dispelled¹. Mature articular cartilage cannot heal spontaneously owing to its low mitotic activity, which contrasts to the rapid rate of chondrocytic mitosis during normal cartilage growth.

Recently, several researchers have attempted to utilize culture-expanded autologous chondrocytes in combination

with collagen sponges or fibrin glue to effect the repair of cartilage defects^{2,3}. However, the results were either unsatisfactory or, if satisfactory, were achieved only after a lengthy wait for the regeneration of hyaline cartilage^{2,4}. These poor results may reflect the characteristics of the transplantation technique, which involves the application of cartilage-derived cells to the defect⁵.

Mesenchymal stem cells (MSCs) isolated from bone marrow have the ability to differentiate into chondrocytes, osteoblasts and other connective tissue cells of mesenchymal origin when cultured under appropriate *in vitro* conditions^{6,7}. In an effort to exploit the pluripotentiality of MSCs, MSC-based repair strategies have been instigated in rabbits and goats, but with limited success^{8,9}. Clinically,

*Address correspondence and reprint requests to: Hideki Yoshikawa. Tel: 81-6-6879-3552; Fax: 81-6-6879-3559; E-mail: yhideki@ort.med.osaka-u.ac.jp

Received 8 November 2004; revision accepted 20 December 2004.

surgical interventions, such as microfracturing, abrasion arthroplasty and osteochondral drilling, have been widely used and considered to be partially successful^{10,11}. These techniques are based on the concept that intentional damage to the subchondral bone recruits MSCs to the defect, thereby promoting cartilage repair.

A potentially powerful alternative approach for cartilage regeneration is the local administration of bone morphogenetic proteins (BMPs), which are members of the transforming growth factor- β superfamily. BMPs have been shown to regulate and promote the growth and differentiation of chondrocytes, osteoblasts and MSCs^{12,13}. Indeed, recombinant human bone morphogenetic protein-2 (rhBMP-2) can stimulate the *in vitro* synthesis of components of the chondrocytic matrix, such as proteoglycans and type-II collagen^{14–16}. Furthermore, BMPs are known to induce the condensation of MSCs when administered *in vivo*^{17–19}.

Inorganic biomaterials, such as carbon fibers²⁰, collagen scaffolds^{2,21}, absorbable polymers^{22,23}, and hydroxyapatite^{24,25}, have been used for articular cartilage repair. Some success has been achieved in the repair of small osteochondral defects, but no widely accepted method exists for the complete healing of hyaline cartilage. The cause of the failure lies not in the nature of the biomaterial itself but in its structure, which is not regulated three-dimensionally.

In the present study, we attempted to combine two distinct approaches: the strong induction of subchondral bone regeneration, with a view to recruiting bone-marrow MSCs to the osteochondral defect; and the appropriate local delivery of rhBMP-2 to induce chondrocytic differentiation and to stimulate matrix production by the chondrocytes. To instigate these two approaches simultaneously, we developed a combined biomaterial, which consists of a synthetic hydroxyapatite with an interconnected porous structure (IP-CHA), and a synthetic bioabsorbable polymer, namely, PLA-PEG (poly-D,L-lactic acid-polyethylene glycol block copolymer). In this system, PLA-PEG serves as a drug-delivery carrier, which permits the ideal release of rhBMP-2 over a period of about 3 weeks^{26–29}. IP-CHA is made from hydroxyapatite, which is a bioactive ceramic with osteoconductive properties^{30,31}. In addition, IP-CHA has a finely organized, three-dimensional interconnecting pore structure. The material is highly porous (porosity: 75%) and the pore size (150 μm) is appropriate for bone formation. The large interconnecting channels (average diameter: 40 μm) permit the easy penetration of tissue into the deep pores³⁰. Owing to these structural properties, IP-CHA can itself induce local bone repair processes^{30,32,33}. The interconnecting pore structure of the material also permits its easy impregnation with cytokines or growth factors borne by an appropriate delivery system.

The rationale behind the selection of key experimental design parameters was as follows: Skeletally immature adolescent rabbits (4–6 months old and 2.5–3.0 kg in weight) were selected because the ability of articular cartilage to repair depends mostly on the bone-marrow MSCs, which are metabolically more active and have a higher capacity to induce repair in an immature model. The decision to use full-thickness defects with a diameter of 4 mm and a depth of 6 mm was based on the results of previous studies. In rabbits, partial-thickness defects do not heal spontaneously, whereas full-thickness ones with a diameter less than 3 mm do, and the repair tissue is composed either of hyaline- or of fibrocartilage^{34–36}. Hence, it was necessary to establish a model in which this upper limit for spontaneous repair was exceeded.

In the present study, we demonstrate the capacity of the triple composite of rhBMP-2, PLA-PEG, and IP-CHA to effect articular cartilage repair. The goal was to achieve the repair of full-thickness articular cartilage defects in rabbits in as short a time as possible, with the ultimate view of inducing the repair of similar lesions in humans; specifically, those generated during osteoarthritis, rheumatoid arthritis, and osteochondritis dissecans.

Materials and methods

PREPARATION OF IMPLANTS

IP-CHA was synthesized by Toshiba Ceramics Co., Ltd. (Kanagawa, Japan), as previously described³⁰. In short, we adopted a "foam gel" technique, which involves two unique steps: a foaming step and a crosslinking step. During the foaming step, the hydroxyapatite slurry is mixed with a foaming agent (polyethyleneimine, 40% by weight). During the crosslinking (polymerization) step, the foam-like hydroxyapatite slurry is rapidly gelatinized using a water-soluble crosslinking agent (a poly-functional epoxy compound)³⁰.

rhBMP-2, which is produced by the Genetics Institute (Cambridge, MA) and was given to us by Yamanouchi Pharmaceutical Co., Ltd. (Ibaraki, Japan), was dissolved in buffer (5 mM glutamic acid, 2.5% glycine, 0.5% sucrose, and 0.01% Tween 80) at a concentration of 1 mg/ml. The solution was then filter-sterilized. Two-hundred mg of PLA-PEG [molecular weight (MW) = 11,400, dispersity (Mw/Mn) = 1.1 (Taki Chemical Research Laboratory, Kanagawa, Japan)] was dissolved in 1 ml of acetone. To prepare a single implant sample, a 25 μl aliquot of the PLA-PEG mass (5 mg) was mixed with a 20 μl sample of rhBMP-2 (20 μg). The specimen of IP-CHA (4 mm in diameter and 4 mm in height) was immersed in the mixture and the solvent was evaporated in a centrifuge/evaporator. The resulting BMP/PLA-PEG/IP-CHA composite was sterilized with ethylene oxide gas for 24 h on the day preceding implantation.

IN VITRO RELEASE KINETICS OF RHBMP-2

The release of rhBMP-2 from the BMP/PLA-PEG/IP-CHA composite was measured using a quantitative sandwich enzyme immunoassay technique (ANALYZA[®]; BMP-2 immunoassay, TECHNE Co. MN, USA). The dose of rhBMP-2 used in the *in vivo* experiments (20 μg) was chosen for the release study. Twelve BMP/PLA-PEG/IP-CHA composites, which were prepared in the same way as those used for implantation in the rabbit model, were placed within 24-well plates together with 500 μl of phosphate-buffered saline [(PBS) Sigma] and incubated for 21 days at 37°C. The supernatant was removed and replaced with fresh PBS every day. The supernatants removed on days 1, 3, 7, 14 and 21 were analyzed for their concentrations of rhBMP-2 according to the enzyme-linked immunosorbent assay (ELISA) technique. The bioactivity of the composites maintained *in vitro* for 0, 7 and 21 days (four samples per time point) was also assessed (see next section).

IN VIVO BIOASSAY FOR THE BMP/PLA-PEG/IP-CHA COMPOSITE

To assess the biological activity of composites that were maintained *in vitro* for 0, 7 and 21 days, these, as well as

IP-CHAs without rhBMP-2 (controls), were implanted within the back muscles of 5-week-old male JCL: ICR mice (one composite per animal; four mice per group, i.e., control, day 1, day 7 and day 21) as previously reported^{27,28}. The implants were harvested 2 weeks after implantation. They were then crushed, homogenized in 0.2% Nonidet P-40 containing 1 mM MgCl₂, and centrifuged at 10,000 rpm for 1 min at 4°C. The supernatants were assayed for alkaline phosphatase (ALP) activity using *p*-nitrophenyl phosphate as a substrate. The product was measured spectrophotometrically at an absorption wavelength of 410 nm (*n* = 4 per group)³⁷.

ANIMAL EXPERIMENTS

Fifty-two New Zealand White rabbits weighing 2.5–3.0 kg (4–6 months) were kept in cages and had free access to food pellets and water. The rabbits were anesthetized by the intravenous injection of 1 ml of pentobarbital [50 mg/ml (Nembutal®; Daiippon Pharmaceutical Co. Ltd., Osaka, Japan)] and the intramuscular injection of 1 ml of xylazine hydrochloride [25 mg/ml (Seractal®; Bayer, Germany)]. After shaving, disinfection, and draping, a straight 3-cm long medial parapatellar incision was made over the right knee and the patella was everted. Full-thickness articular osteochondral defects, 4 mm in diameter and 6 mm in depth, were created mechanically in the patellar groove of the right distal femur. Rabbit knees were divided into four implant groups: group I (*n* = 16 knees) received the BMP/PLA-PEG/IP-CHA composite; group II (*n* = 12 knees) received the PLA-PEG/IP-CHA composite (no rhBMP-2), group III (*n* = 12 knees) received IP-CHA alone; and group IV (*n* = 12 knees) underwent a sham operation with no implantation. In groups I, II, and III, all implants were placed at the subchondral bone level, 2 mm beneath the surface of the adjacent cartilage. The fascial layer was closed with absorbable sutures, and the skin with 4-0 nylon sutures. One week after surgery, four rabbits in group I were killed. At 3 weeks, 24 rabbits were killed (group I = 6, group II = 6, group III = 6, group IV = 6), and at 6 weeks 24 rabbits were killed (group I = 6, group II = 6, group III = 6, group IV = 6). The animals were killed by an intravenous injection of 5 ml of pentobarbital (Table I). All animal experiments were approved by the Animal Laboratory, Faculty of Medicine, Osaka University, Japan.

RADIOGRAPHIC AND HISTOLOGICAL EVALUATIONS

The harvested tissues were radiographed using a soft X-ray apparatus [35 kV; 300 μA; 300 s; MX20 (Faxitron

Table I
Information respecting the deployment of the 52 rabbits used in this study

	Number of rabbits				Total number
	Group I	Group II	Group III	Group IV	
Materials					
IP-CHA	+	+	+	-	
rhBMP-2	+	-	-	-	
PLA-PEG	+	+	-	-	
Follow-up time					
1 week	4	0	0	0	4
3 weeks	6	6	6	6	24
6 weeks	6	6	6	6	24
Total number	16	12	12	12	52

X-ray Co., IL, USA)] and then fixed in 4% paraformaldehyde (pH 7.4) for 48 h at 4°C. Tissue samples were decalcified in 20% ethylenediaminetetraacetic acid (pH 7.4) at 4°C, dehydrated in a graded ethanol series and embedded in paraffin. Serial sections (5 μm in thickness) were cut sagittally through the center of the operative site and stained with hematoxylin and eosin (H&E) or with safranin-O. For the immunohistochemical analysis, paraffin sections were treated with 3% H₂O₂ to block endogenous peroxidase activity. They were pretreated with serum to block non-specific staining. The sections were then incubated with mouse monoclonal antibodies: anti-type-I collagen (I-8H5, Daiichi Fine Chemical Co., Ltd, Toyama, Japan), anti-type-II collagen (II-4C11, Daiichi Fine Chemical Co., Ltd, Toyama, Japan), and anti-CD105 [(Endoglin) 555722, BD Bioscience, NJ, USA]; and with the polyclonal antibody goat anti-Cbfa1 [(Runx2) C-19, Santa Cruz, CA, USA]³⁸. The specimens were treated with the appropriate biotinylated secondary antibodies, and then incubated with the streptavidin/horseradish peroxidase complex. The signal was visualized as the red reaction product of a 3-amino-9-ethyl carbazole liquid substrate chromogen (AEC, DAKO JAPAN Co., Ltd, Kyoto, Japan). To confirm the specificity of

Table II
Histological scoring system*

Category	Points
Cell morphology	
Hyaline cartilage	4
Mostly hyaline cartilage	3
Mostly fibrocartilage	2
Mostly non-cartilage	1
Non-cartilage only	0
Matrix-staining (metachromasia)	
Normal	3
Slightly reduced	2
Markedly reduced	1
No metachromatic staining	0
Structural integrity	
Normal	2
Slight disruption	1
Severe disintegration	0
Surface regularity†	
Smooth	3
Moderate	2
Irregular	1
Severely irregular	0
Thickness of cartilage, %	
121–150	1
81–120	2
51–80	1
0–50	0
Regenerated subchondral bone	
Good	2
Moderate	1
Poor	0
Integration with adjacent cartilage	
Both edges integrated	2
One edge integrated	1
Neither edge integrated	0
Total maximum	18

*A modified version of the system described by Wakitani *et al.*⁸.
†Total smooth area of repair cartilage compared with the entire area of the cartilaginous compartment of the defect.

the antibody under the adopted conditions and to confirm the specificity of the markers in target cells, all antibodies were tested for their reactivity in control tissues.

HISTOLOGICAL SCORING

To quantify the histological repair of articular cartilage defects, we employed a modified version of the grading scale described by Wakitani *et al.*⁹ This consists of seven categories and assigns a score ranging from 0 to 18 points (Table II). The following parameters were assessed: cell morphology (hyaline cartilage); metachromatic staining of the cartilage matrix; structural integrity of the regenerated cartilage; surface regularity of the tissue; thickness of the cartilage layer; regeneration of the subchondral bone; and integration of the tissue with adjacent cartilage.

STATISTICAL ANALYSES

Data pertaining to ALP activity were analyzed using an unpaired Student's *t* test. The histological scoring data were analyzed using the Kruskal–Wallis test, with a *post hoc* Bonferroni correction for non-parametric data.

Results

EVALUATION OF THE IMPLANTS

Scanning electron microscopy of IP-CHA samples revealed these to have a finely organized three-dimensional structure. Most of the IP-CHA pores were spherical, of similar size (approximately 100–200 μm in diameter) and uniformly interconnected via channels [10–80 μm in diameter; Fig. 1(B, C)]. Scanning electron microscopy of the BMP/PLA–PEG/IP-CHA composite revealed the BMP/PLA–PEG component to affect neither the pore size nor

the interconnecting pore structure and to coat well the surface of the IP-CHA [Fig. 1(D, E)].

IN VITRO RELEASE KINETICS OF rhBMP-2 AND IN VIVO BIOASSAY FOR THE BMP/PLA–PEG/IP-CHA COMPOSITE

Based on ELISA, the BMP/PLA–PEG/IP-CHA composite released significant quantities of rhBMP-2 during the 21-day monitoring period [$6.85 \pm 1.31 \mu\text{g/ml}$ on day 1, $0.79 \pm 0.22 \mu\text{g/ml}$ on day 3, $22.9 \pm 0.62 \text{ ng/ml}$ on day 7, $4.76 \pm 1.13 \text{ ng/ml}$ on day 14, and $2.71 \pm 0.70 \text{ ng/ml}$ on day 21; Fig. 2(A)].

To assess the bioactivity of the BMP/PLA–PEG/IP-CHA composites maintained *in vitro* for 0, 7 or 21 days, we implanted these, as well as IP-CHAs (control for the absence of rhBMP-2) within the back muscles of male ICR mice (a standard ectopic bone-formation model) and then analyzed the explanted material for its ALP activity. High levels of ALP activity could be detected even on day 21 [Fig. 2(B)], which accords with the rhBMP-2 release kinetics results *in vitro*.

MACROSCOPIC OBSERVATIONS OF CARTILAGE DEFECTS

Three weeks after implantation, the repaired defects in group I had a macroscopically smooth and glistening appearance and exhibited continuity with the surrounding host cartilage [Fig. 3(A)]. The controls (groups II–IV) revealed varying degrees of cartilage resurfacing with fibrous tissue [Fig. 3(B–D)].

At 6 weeks, the color and the glistening appearance of the repaired defects in group I were similar to those manifested by the adjacent host cartilage. The junction between the repaired tissue and the surrounding host cartilage was not clearly visible [Fig. 3(E)]. In contrast, the regenerated tissue in the control groups (groups II–IV) was

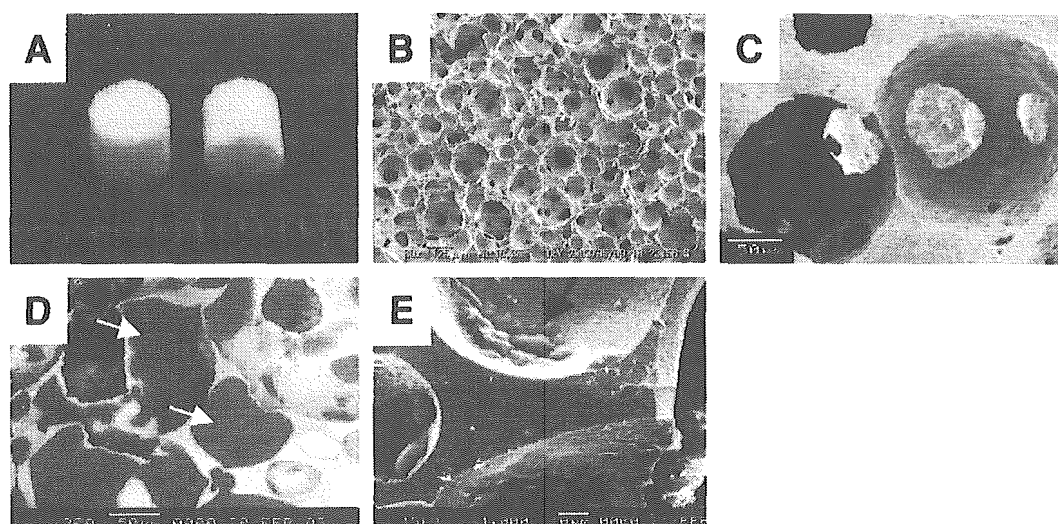


Fig. 1. Macroscopic photograph (A) and scanning electron micrographs (B–E) of IP-CHA specimens (4 mm in diameter and 4 mm in height). (A) Macroscopically, the surface of IP-CHA is slightly rough compared with that of other commercial porous hydroxyapatite materials, owing to its regular porous structure. (B, C) Scanning electron micrographs of IP-CHA, illustrating the regular arrangement of pores which are of similar size (100–200 μm in diameter), uniformly connected with each other, and separated by thin walls. (B) = 80 \times ; (C) = 600 \times . (D, E) Scanning electron micrographs of the BMP/PLA–PEG/IP-CHA composite. (D) The dark areas lining the pores (white arrows) represent the BMP/PLA–PEG component. The introduction of BMP/PLA–PEG had no effect on either the pore size or the interconnecting pore structure. (E) Higher magnification of the lining of a pore (black arrow), revealing it to be well coated with BMP/PLA–PEG. (D) = 300 \times ; (E) = 1000 \times .

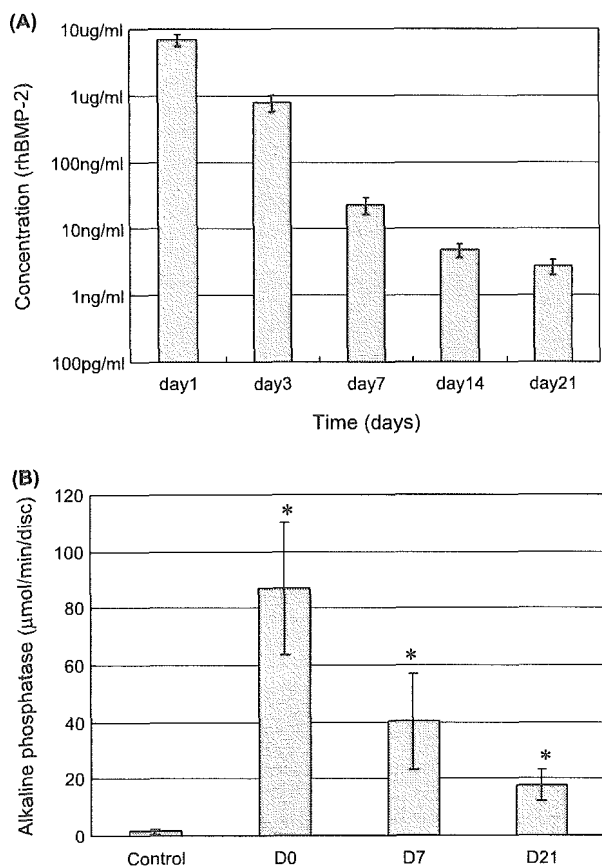


Fig. 2. Time course of rhBMP-2 release from the BMP/PLA-PEG/IP-CHA composite *in vitro* (A) and the bioactivity of the composites *in vivo* (B). (A) Release kinetics (measured by ELISA) of rhBMP-2 from the BMP/PLA-PEG/IP-CHA composite, illustrating significant quantities of rhBMP-2 during the 21-day monitoring period. The bar graph depicts the non-cumulative release at each time point. Mean values \pm SD ($n = 4$) are represented. (B) The bioactivity of BMP/PLA-PEG/IP-CHA composites that were maintained *in vitro* for 0 (D0), 7 (D7), or 21 (D21) days was assessed 2 weeks after their implantation at an ectopic site in mice by monitoring the ALP activity of the explanted material. PLA-PEG/IP-CHA (no rhBMP-2) represented the control. High levels of ALP activity could be detected even on day 21 [86.8 ± 23.2 $\mu\text{mol}/\text{min}/\text{disc}$ (day 0), 40.3 ± 16.8 $\mu\text{mol}/\text{min}/\text{disc}$ (day 7), 17.7 ± 5.2 $\mu\text{mol}/\text{min}/\text{disc}$ (day 21), 1.6 ± 0.8 $\mu\text{mol}/\text{min}/\text{disc}$ (control)]. Mean values \pm SD ($n = 4$) are represented. * = value is significantly different from the control ($P < 0.05$).

fibrous, and had a rough surface containing many fissures [Fig. 3(F-H)].

RADIOGRAPHIC EVALUATION

Six weeks after implantation, the soft X-ray analysis revealed defects treated with the BMP/PLA-PEG/IP-CHA composite (group I) to be consistently filled with newly formed bone, which was continuous with the surrounding intact subchondral bone [Fig. 3(I)]. In the control groups (groups II-IV), bone formation was incomplete and irregular [Fig. 3(J-L)].

HISTOLOGICAL EVALUATION

One week after implantation with the BMP/PLA-PEG/IP-CHA composite (group I), vigorous new bone formation

was observed histologically within the pores of the IP-CHA scaffold [Fig. 4(B)], and about three-quarters of the defect depth above the IP-CHA had already been replaced with repair tissue. The central part of the repair tissue contained a fibrin clot and a few vessels. The lateral and lower regions consisted of granulation tissue, which was actively undergoing neovascularization and contained rounded fibroblast-like cells. These cells registered positive for Cbfa1 and/or CD105. They appeared to have infiltrated from the surrounding intact subchondral bone, either directly, or indirectly via the interconnecting IP-CHA pores, which were likewise filled with granulation tissue. Some of the pores in the peripheral 1-mm portions of IP-CHA blocks already contained newly formed bone (Fig. 4).

Three weeks after implantation with BMP/PLA-PEG/IP-CHA, the defect space above the IP-CHA blocks (subchondral space) was filled with newly generated and vigorous bone tissue, which penetrated the interconnecting pores of this material [Fig. 5(A, F)]. The regenerated articular cartilage was more cellular and contained less extracellular matrix than normal cartilage. The regenerated cartilage was divided into three distinct zones: (1) a superficial one, which contained flattened hyperchromatic cells; (2) a middle one, which contained rounded chondrocytes; and (3) a zone of enchondral ossification. The cartilage-like layer was two-to-three times thicker than normal cartilage [Fig. 5(A, E)]. In each of the control groups (groups II-IV), the regenerated fibrous cartilage had a similar morphological appearance, irrespective of the absence or presence of an implant. Although the subchondral space in group II tended to be filled with more newly formed bone than did that in the other control groups (groups III and IV), the quantitative histological evaluation revealed no significant difference between them [Table III; Fig. 5(B-D)].

Six weeks after implantation, defects treated with the BMP/PLA-PEG/IP-CHA composite (group I) were filled with regenerated subchondral bone, which also penetrated the pores of the implant. The subchondral bone was covered with a layer of regenerated cartilage tissue of almost normal thickness. The hyaline nature of the cartilage was maintained, and the tissue was beginning to assume a columnar organization and a horizontal stratification into four distinct zones (superficial, middle, deep and calcified), as in normal cartilage [Fig. 6(A, E)]. Interestingly, no gaps could be distinguished microscopically between the host cartilage and the newly regenerated cartilage, which suggests that the tissues were functionally and biologically integrated [Fig. 6(F)]. Safranin-O staining was evident predominantly in the middle and deep zones. Immunoreactivity for type-II collagen tended to be weakest in the deep zone at the junction with host tissue. But generally, the matrix exhibited a hyaline-like cartilaginous phenotype [registering negative for type-I collagen; Fig. 6(J-L)]. In contrast, defects in the control groups (groups II-IV) were filled with a hypercellular type of fibrous tissue. No hyaline cartilage was detected, despite the presence of new bone above and within the implant; [Fig. 6(B-D, G-I)]. Histological sections were assessed quantitatively using a modified version of an established grading system, which measures the degree and quality of cartilage repair⁸ (Table II). At each time point, the scores for the BMP/PLA-PEG/IP-CHA composite (group I) were significantly better than those for groups II, III and IV ($P < 0.01$). These findings accord with the macroscopic and histological observations.

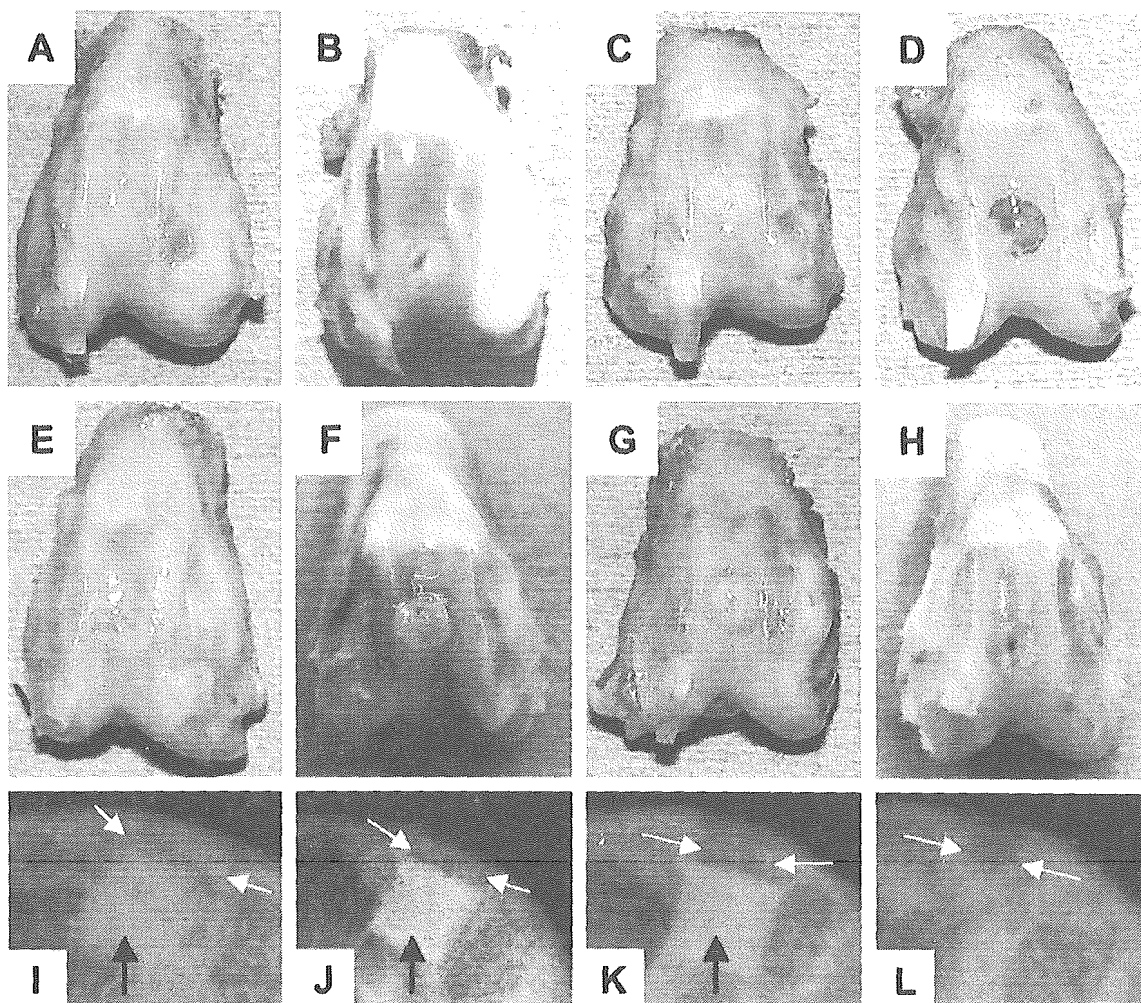


Fig. 3. Gross appearance (A–H) and soft X-ray photographs (I–L) of four specimens (one in each group) 3 weeks (A–D) and 6 weeks (E–L) after implantation. (A, E, I): BMP/PLA–PEG/IP-CHA composite (group I). (B, F, J): PLA–PEG/IP-CHA composite (group II). (C, G, K): IP-CHA alone (group III). (D, H, L): no implant (group IV). (A, E) In group I, reconstruction of the surface was good. At 3 weeks, the surface was still a little “white”; but at 6 weeks, it was smooth and glistening and exhibited continuity with the surrounding intact host cartilage. These macroscopic findings correspond with the histological results (Table III). (B, F) In group II, the articular cartilage defects were covered with “white” fibrous tissue with many fissures. (C, G) In group III, the regeneration of the defect looked better than those of other control groups (group II and IV), whereas the junction of the defects were still visible. (D, H) In group IV, in which the defects were left empty, at 3 weeks the defects were filled with irregular “white” tissue with pin-hole like fissure (H). (I–L) Representative soft X-ray photographs of the four specimens. The black arrows denote the implanted IP-CHA block. The white arrows above the IP-CHA block indicate the region where subchondral bone should be regenerated. A white, radiodense zone was observed above the IP-CHA block in group I (I); it denotes a vigorous regeneration of subchondral bone. This radiodense zone was not detected in groups II–IV (J–L).

Discussion

Several investigators have reported on the repair of articular cartilage defects using diverse tissue-engineering approaches. These include a gene-enhanced technique, the direct implantation of growth factors, and *in vitro* cell expansion^{39–42}. BMPs have been shown to induce the differentiation of MSCs into chondrocytes both *in vitro* and *in vivo*. BMPs (BMP-2 and BMP-7) have also been used in conjunction with type-I collagen sponges to elicit the repair of osteochondral defects^{43–45}. Cook *et al.*⁴⁰ have reported that type-I collagen sponges impregnated with rhBMP-7 can induce the repair of full-thickness osteochondral defects

with hyaline-like cartilage in a dog model. The hyaline-like quality of the repair cartilage was still evident 52 weeks after surgery and the tissue had undergone no significant degradation. Sellers *et al.*⁴¹ have demonstrated the capacity of rhBMP-2 to accelerate the healing of full-thickness articular cartilage defects and to improve the histological appearance and the biochemical characteristics of the repair cartilage. However, the tissue still differed from normal hyaline cartilage, both biochemically and structurally, and a long time elapsed before the defect area was completely filled with it. These suboptimal results probably reflect a limited recruitment of MSCs and/or a restricted delivery of cytokines, owing to the poor structural

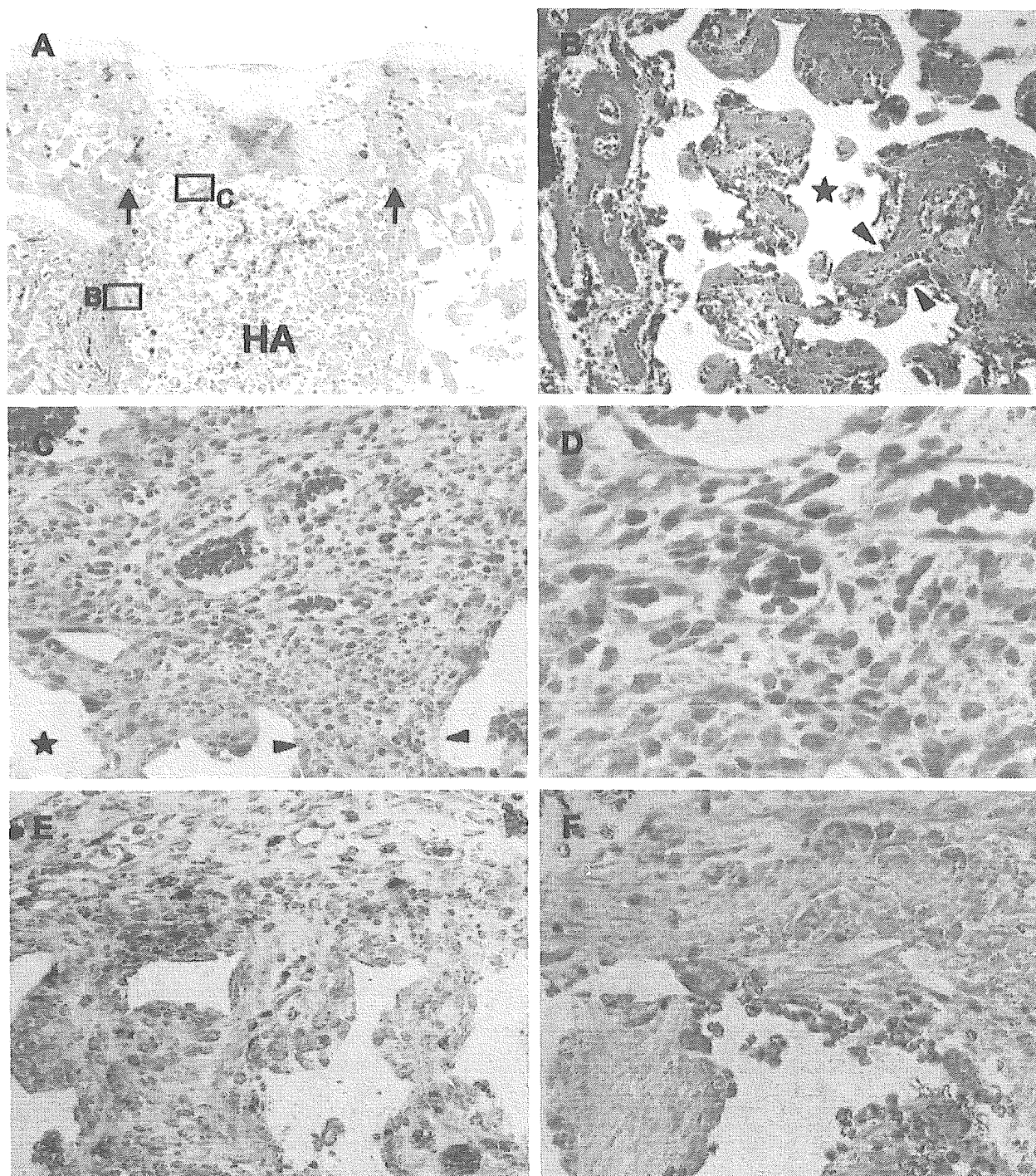


Fig. 4. Histological photomicrographs of a defect 1 week after the implantation of a BMP/PLA-PEG/IP-CHA composite (group I). (A) Overview of the defect site, the margins of which are indicated by arrows. HA represents the implanted IP-CHA scaffold (H&E). (B) Higher magnification of the region indicated in (A). The surface of newly formed bone trabeculae are lined with numerous cuboidal osteoblasts which have migrated from the neighboring host bone. (C) Higher magnification of the region indicated in (A), illustrating a neovascularized aggregate of cells which have migrated from the neighboring bone marrow, either directly or indirectly via the interconnecting channels of the IP-CHA composite. The arrowheads in (B) and (C) indicate the interconnecting pores of the IP-CHA scaffold. The asterisks denote regions that were occupied by hydroxyapatite before decalcification. (D) Higher magnification of (C), illustrating the rounded, fibroblast-like form of the aggregated cells. (E, F) Immunostaining of the aggregated cells for Cbfa1 (E) and CD105 (F). Many of the cells expressed the chondro/osteoblastic marker (E) and/or the mesenchymal one (F). Magnification: (A) = 10 \times ; (B, C) = 100 \times ; (E, F) = 200 \times ; (D) = 400 \times .

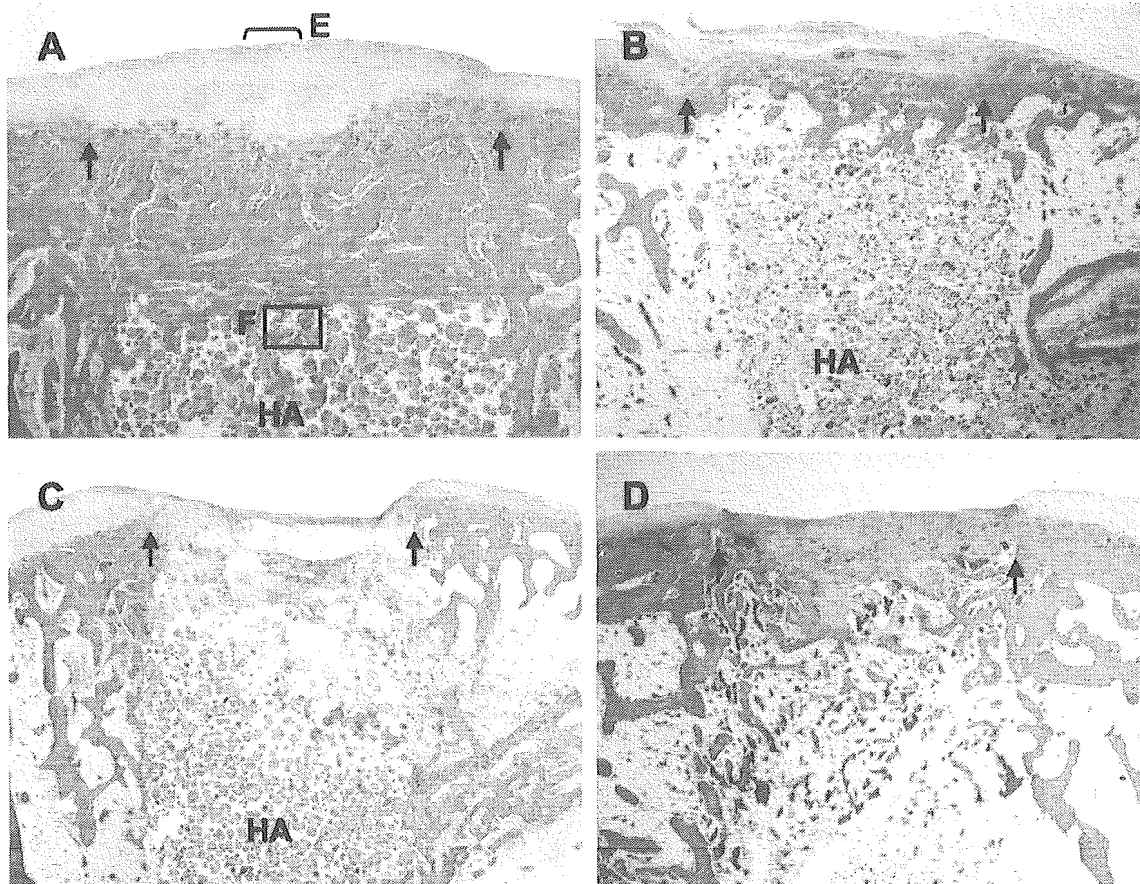


Fig. 5. Histological photomicrographs of defects (H&E staining) 3 weeks after implantation with either the BMP/PLA-PEG/IP-CHA composite [(group I) A, E, F], the PLA-PEG/IP-CHA composite [(group II) B], or IP-CHA alone [(group III) C], and in the absence of treatment [empty (group IV) D]. Arrows indicate the margins of the defect. HA represents the implanted IP-CHA scaffold. Highly magnified images of the regions indicated in (A) are represented in (E) and (F). (A) Section of a defect filled with the BMP/PLA-PEG/IP-CHA composite (group I), illustrating well-organized hyaline-like cartilage and accelerated replacement of vigorous subchondral bone. (B–D) In each of the control groups (group II–IV), the regenerated tissue had a similar morphological appearance, irrespective of the absence or presence of an implant. The defect site was filled predominantly with a hypocellular fibrocartilage repair tissue with incomplete replacement of subchondral bone. (E) The regenerated articular cartilage was more cellular and contained less extracellular matrix than normal cartilage. However, a stratified structure similar to normal cartilage was already visible. (F) Vigorous regeneration of subchondral bone occurred, which was carried up through the interconnections of the IP-CHA scaffold (arrowheads). The asterisk denotes a region that was occupied by hydroxyapatite before decalcification. Magnification: (A–D) = 10 \times ; (E, F) = 100 \times .

organization of the supporting scaffold. The purpose of the present study was to evaluate the potential of IP-CHA to serve as a scaffold for the repair of full-thickness articular cartilage defects. This material has a well-organized inter-pore connectivity.

The osteoconductivity of polymer implants containing rhBMP-2 has been studied extensively^{28,46}. In the present study, we used the synthetic bioabsorbable polymer PLA-PEG as a carrier for rhBMP-2. *In vitro*, rhBMP-2 was released continuously from the BMP/PLA-PEG/IP-CHA composite over a period of 21 days, as determined by ELISA [Fig. 2(A)]. This finding accords with the results of the *in vivo* bioassay [Fig. 2(B)], which was based on the ALP activity of composites implanted at an ectopic site in mice. However, it is of course conceivable that the release profile of rhBMP-2 at this ectopic site in mice differs greatly from that at the orthotopic site in our rabbit model.

Our new strategy for articular cartilage repair appears to be unique in three respects: (1) autogenous MSCs were

efficiently recruited from the bone marrow by strongly activating regeneration within the subchondral bone compartment of the defect; (2) a sustained BMP stimulus appears to promote not only the vigorous regeneration of subchondral bone but also the ensuing differentiation of chondrocytes and the production of a cartilaginous matrix at the surface, which results in the regeneration of a hyaline-like cartilage layer in as short a time as 3 weeks; and (3) the regenerated cartilage integrated almost perfectly with the surrounding host cartilage, probably because the entire regeneration process was conducted *in situ*, i.e., it did not involve an *in vitro* chondrocyte-culturing step.

It is not known why the thickness of the repaired articular cartilage corresponded so closely to that of the host articular cartilage, with no bony differentiation. But articular factors, such as oxygen tension, joint effusion and mechanical stress, as well as subchondral influences, may regulate the differentiation process. Although the regenerated cartilage present 6 weeks after surgery was

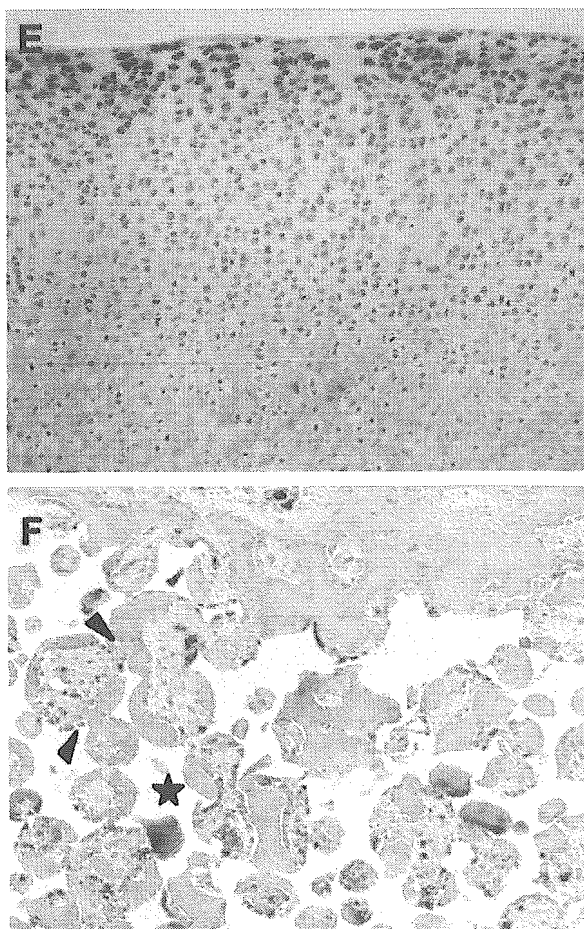


Fig. 5. (continued).

microscopically so well integrated with the surrounding host cartilage, the histological analysis revealed a slight discrepancy between safranin-O staining and immunoreactivity for type-II collagen [Fig. 6(J, L)]. This may be accounted for by the fact that chondrocytes near the junction with host cartilage produced less matrix than did those located more centrally within the regenerated tissue, where staining with

safranin-O was absent only from the superficial zone, as in normal articular cartilage.

Cbfa1, a member of the Runt-domain family of transcriptional factors, is expressed not only in all osteoblasts, but also in chondrocytes and in earlier prechondrogenic mesenchymal condensations⁴⁷⁻⁴⁹. Furthermore, Cbfa1 is known to play an essential role in the differentiation not only of osteoblasts but also of chondrocytes, both at an early and a later stage of the process^{50,51}. CD105 is a putative cell-surface marker for MSCs, which have the ability to undergo chondrogenesis, osteogenesis and adipogenesis^{52,53}. One week after implantation, numerous cuboidal osteoblasts migrated into the pores of the IP-CHA scaffold from the host bone marrow (Fig. 3). And within peripheral pores, they had already begun to form bone tissue. The subchondral space above the IP-CHA scaffold was filled with an agglomeration of rounded fibroblast-like cells, which registered positive for Cbfa1 and/or CD105. They appeared to have migrated from the adjacent bone marrow, either directly, or indirectly via the interconnecting pores of the IP-CHA. These findings suggest that the aggregating fibroblast-like cells might have the potential for chondro/osteogenesis.

According to our findings, one of the keys to successful articular cartilage regeneration might be the activation of a subchondral repair process, thereby enabling chondroblastic/osteoblastic cells to effectively aggregate within the subchondral space. In rabbits, small, 3-mm-diameter, full-thickness articular cartilage defects heal spontaneously with repair tissue, which is composed of hyaline-like or fibrous cartilage. In adolescent rabbits (approximately 3 months old), osteochondral defects repair better and more rapidly than do those in adults^{34,54}. Furthermore, adolescent rabbits have a larger population of metabolically active bone-marrow MSCs. Hence, in the present study, we established a large (4-mm-diameter) full-thickness defect model, it being necessary to exceed the upper limit (3 mm in diameter) for spontaneous repair. And since our system involved no cell-expansion step *in vitro*, the adolescent (rather than the adult) rabbit model was considered to be advantageous in its possession of a larger population of metabolically active bone-marrow MSCs.

A basic requirement for biomaterials is that they be non-carcinogenic and elicit no inflammatory reaction due to cytotoxicity or immunogenicity⁵⁵. The BMP/PLA-PEG/IP-CHA composite is believed to meet these criteria. The PLA and PEG homopolymers and hydroxyapatite have been shown to be compatible and safe for clinical applications^{30,56}. In addition to these safety features, it is crucial that biomaterials are easy to handle in clinical settings.

Table III
Results of the histological scoring

Group	No. of defects	Cell morphology	Matrix-staining	Structural integrity	Surface regularity	Thickness	Reconstruction of subchondral bone	Integration with adjacent cartilage	Total score
Group I: 3 weeks	6	3.6 ± 0.5*	2.0 ± 0	1.3 ± 0.5	2.0 ± 0.9	1.2 ± 0.4	0.8 ± 0.7	1.8 ± 0.4§	12.8 ± 2.4*
Group II: 3 weeks	6	1.7 ± 0.5	1.0 ± 0.6	0.5 ± 0.5	0.5 ± 0.5	0.7 ± 0.5	0.5 ± 0.4	1.0 ± 0.6§	5.8 ± 2.6
Group III: 3 weeks	6	2.2 ± 0.8	1.3 ± 0.5	0.5 ± 0.5	0.7 ± 0.4	1.0 ± 0	0.5 ± 0.4	1.2 ± 0.8§	7.2 ± 2.2
Group IV: 3 weeks	6	1.3 ± 0.5	0.8 ± 0.4	0.7 ± 0.5	1.3 ± 0.5	0.5 ± 0.3	0.5 ± 0.3	0.5 ± 0.3	5.1 ± 1.1
Group I: 6 weeks	6	3.8 ± 0.4*	2.3 ± 0.5*	1.5 ± 0.5§	2.2 ± 1.0	1.2 ± 0.4§	1.8 ± 0.4§	1.5 ± 0.5	15.0 ± 2.1*
Group II: 6 weeks	6	1.8 ± 0.4	1.5 ± 0.5	1.2 ± 0.4	1.5 ± 0.5	1.2 ± 0.4	1.3 ± 0.5§	1.2 ± 0.4	9.7 ± 1.2
Group III: 6 weeks	6	1.7 ± 1.0	1.0 ± 0.8	0.8 ± 0.4	1.7 ± 0.5	0.7 ± 0.5	1.3 ± 0.5§	1.2 ± 0.4	8.3 ± 3.0
Group IV: 6 weeks	6	1.5 ± 0.5	0.5 ± 0.4	0.5 ± 0.5	1.3 ± 0.5	0.7 ± 0.5	0.5 ± 0.3	0.8 ± 0.4	5.7 ± 1.9

Values represent the average score ± SD for each category. **P* < 0.01 vs groups II, III, and IV. §*P* < 0.01 vs group IV.

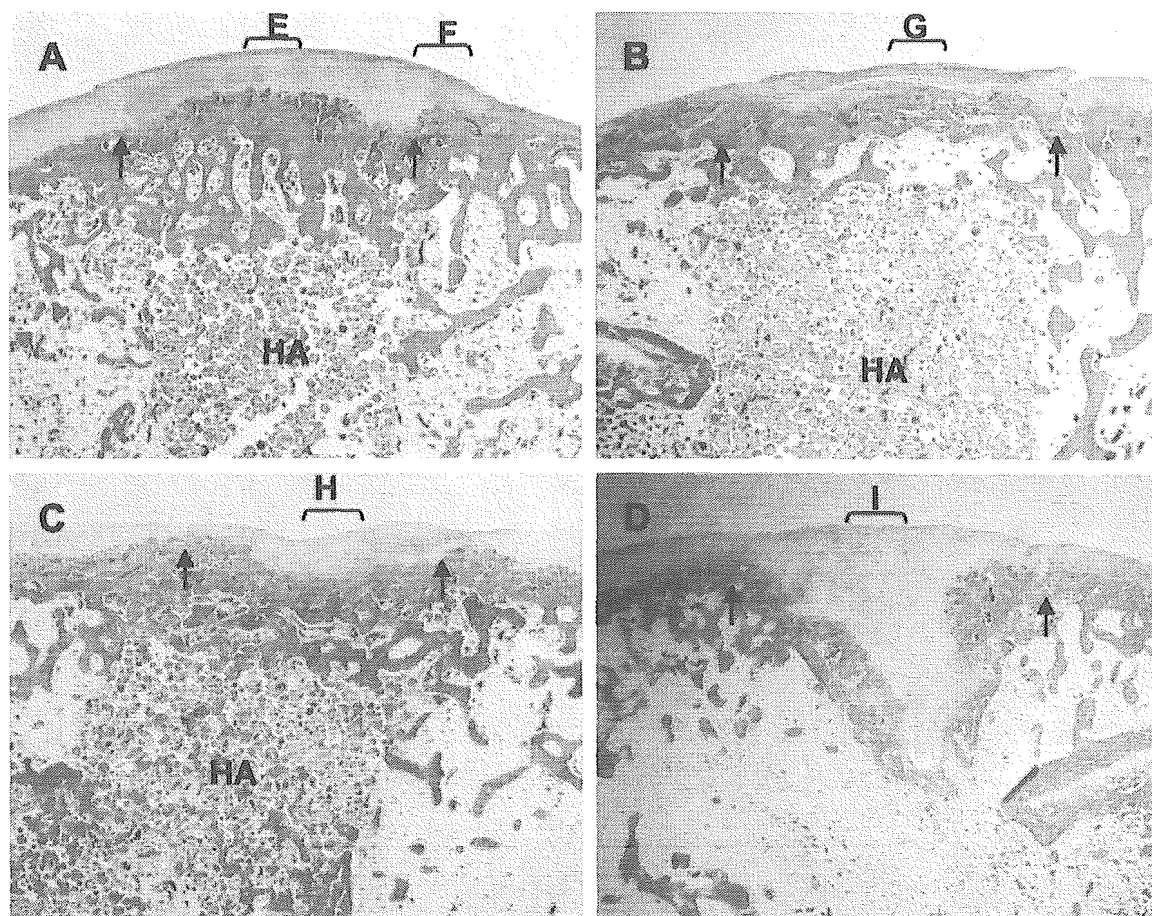


Fig. 6. Histological photomicrographs of defects 6 weeks after implantation with either the BMP/PLA-PEG/IP-CHA composite [(group I) A, E, F, J-L], the PLA-PEG/IP-CHA composite [(group II) B, G], or IP-CHA alone [(group III) C, H], and in the absence of treatment [empty (group IV) D, I]. Arrows indicate the margins of the defect. HA represents the implanted IP-CHA scaffold. Highly magnified images of the regions indicated in (A-D) are represented in (E-I). (A) The defect treated with the BMP/PLA-PEG/IP-CHA composite (group I) was filled with regenerated subchondral bone, which also penetrated the pores of the implant. The subchondral bone was covered with a layer of regenerated cartilage tissue of almost normal thickness. (B, C) In the control groups (group II and III), the defects were filled with a hypercellular type of fibrous tissue with regeneration of subchondral bone. The surface the repaired tissue was rough. (D) Without treatment (group IV), the defect site was predominantly replaced by thick fibrocartilage tissue with a thin layer of irregular subchondral bone. (E) The central region of the regenerated articular cartilage layer (group I). The repaired tissue has a hyaline-like appearance and is undergoing organization into vertical columns. The four horizontal strata characteristic of normal articular cartilage are apparent. (F) The junction between host and regenerated cartilage is continuous, and very little fibrillation of the articular surface is apparent (group I). (G-I) The repaired tissue is mainly of a fibrous nature (group II-IV). (J-L) Safranin-O staining (J), and immunostaining for type-I collagen (K) and type-II collagen (L) at the junction between host and the regenerated cartilage (group I). Magnification: (A-D) = 10 \times ; (E-I) = 100 \times ; (J-L) = 40 \times . (A-I): H&E staining.

Current techniques using cultured chondrocyte suspensions or collagen gels are complicated by problems associated with cell retention. Our composite material circumvents these problems. Furthermore, our material may be shaped into a "ready-to-use" form. It is possible to adjust its size and shape to suit the dimensions of the defect prior to implantation.

In conclusion, we have successfully induced the repair of articular cartilage defects within a relatively short period of time by combining rhBMP-2 with two biomaterials: IP-CHA as a scaffold and PLA-PEG as a carrier for rhBMP-2. The BMP/PLA-PEG/IP-CHA composite represents a new and promising technology for the engineering of articular cartilage. Clinical applications for the treatment of both osteoarthritis and articular cartilage injuries are also

anticipated. Further studies involving long-term observations in both adolescent and adult animals are currently underway.

Acknowledgments

The authors thank Toshiba Ceramics Co., Ltd. for supplying the materials used in this study and for their technical assistance. We also thank Miss K. Asai for her technical assistance. This study was partially supported by grants from the Japanese Ministry of Health and Welfare, the Japanese Ministry of Education, Science and Culture, the Uehara Memorial Foundation, the New Energy and

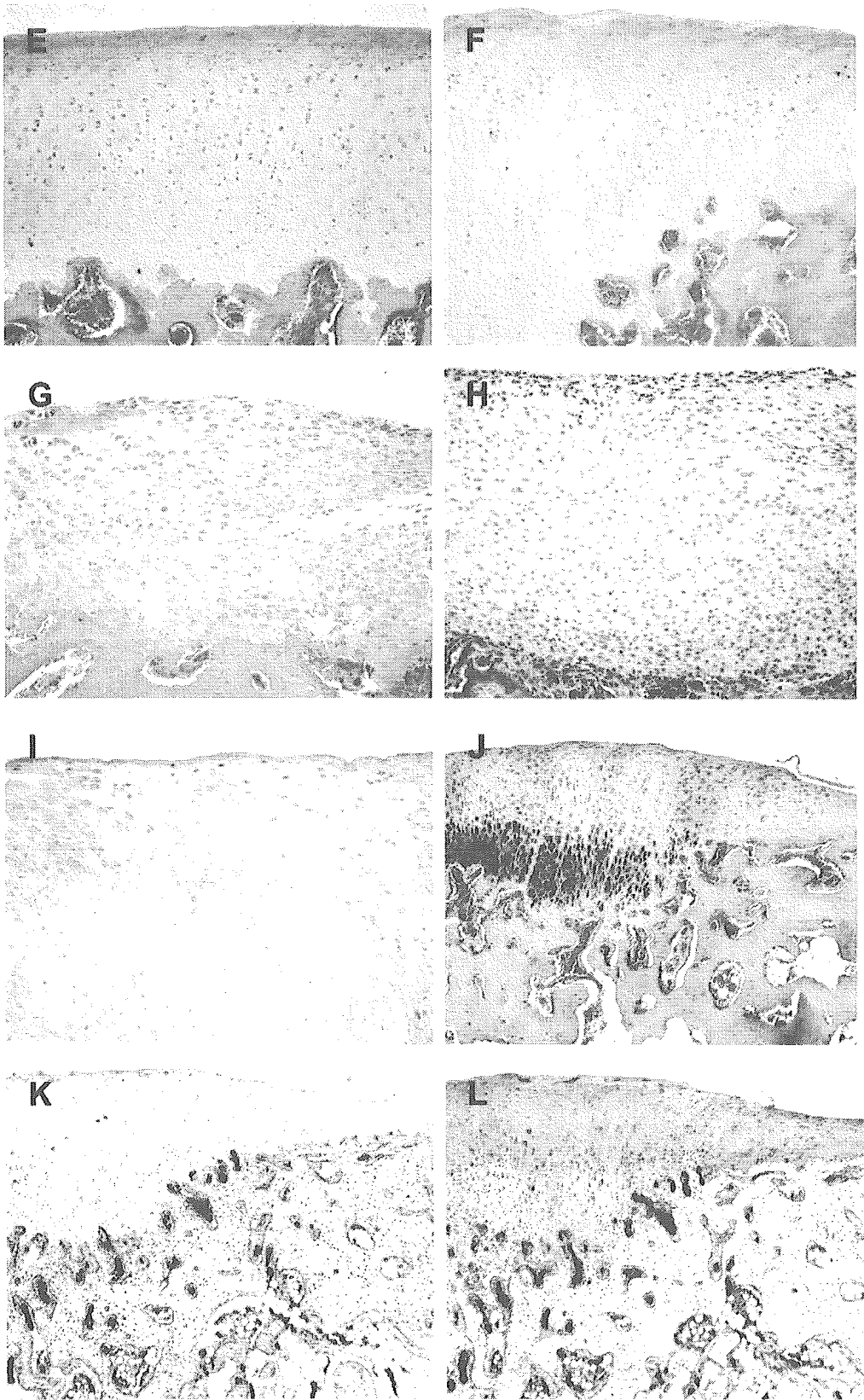


Fig. 6. (continued).

Industrial Technology Development Organization, the Japan Orthopaedics and Traumatology Foundation (No.0122), and JSPS Research Fellowships for Young Scientists (No. 04920).

References

- Newman AP. Articular cartilage repair. *Am J Sports Med* 1998;26:309–24.
- Lee CR, Grodzinsky AJ, Hsu HP, Spector M. Effects of a cultured autologous chondrocyte-seeded type II collagen scaffold on the healing of a chondral defect in a canine model. *J Orthop Res* 2003;21:272–81.
- van Susante JL, Buma P, Homminga GN, van den Berg WB, Veth RP. Chondrocyte-seeded hydroxyapatite for repair of large articular cartilage defects. A pilot study in the goat. *Biomaterials* 1998;19:2367–74.
- Mainil-Varlet P, Rieser F, Grogan S, Mueller W, Saager C, Jakob RP. Articular cartilage repair using a tissue-engineered cartilage-like implant: an animal study. *Osteoarthritis Cartilage* 2001;9:S6–S15.
- Litzke LE, Wagner E, Baumgaertner W, Hetzel U, Josimovic-Alasevic O, Libera J. Repair of extensive articular cartilage defects in horses by autologous chondrocyte transplantation. *Ann Biomed Eng* 2004;32:57–69.
- Pittenger MF, Mackay AM, Beck SC, Jaiswal RK, Douglas R, Mosca JD, *et al.* Multilineage potential of adult human mesenchymal stem cells. *Science* 1999;284:143–7.
- Kadiyala S, Young RG, Thiede MA, Bruder SP. Culture expanded canine mesenchymal stem cells possess osteochondrogenic potential *in vivo* and *in vitro*. *Cell Transplant* 1997;6:125–34.
- Wakitani S, Goto T, Pineda SJ, Young RG, Mansour JM, Caplan AI, *et al.* Mesenchymal cell-based repair of large, full-thickness defects of articular cartilage. *J Bone Joint Surg Am* 1994;76-A:579–92.
- Butnariu-Ephrat M, Robinson D, Mendes DG, Halperin N, Nevo Z. Resurfacing of goat articular cartilage by chondrocytes derived from bone marrow. *Clin Orthop* 1998;330:234–43.
- Steadman JR, Rodkey WG, Rodrigo JJ. Microfracture: surgical technique and rehabilitation to treat chondral defects. *Clin Orthop* 2001;391S:362–9.
- Kumai T, Takakura Y, Higashiyama I, Tamai S. Arthroscopic drilling for the treatment of osteochondral lesions of the tarus. *J Bone Joint Surg Am* 1999;81-A:1229–35.
- Shea CM, Edgar CM, Einhorn TA, Gerstenfeld LC. BMP treatment of C3H10T1/2 mesenchymal stem cells induces both chondrogenesis and osteogenesis. *J Cell Biochem* 2003;90:1112–27.
- Carlberg AL, Pucci B, Rallapalli R, Tuan RS, Hall DJ. Efficient chondrogenic differentiation of mesenchymal cells in micromass culture by retroviral gene transfer of BMP-2. *Differentiation* 2001;67:128–38.
- Zuscik MJ, Baden JF, Wu Q, Sheu TJ, Schwarz EM, Drissi H, *et al.* 5-azacytidine alters TGF-beta and BMP signaling and induces maturation in articular chondrocytes. *J Cell Biochem* 2004;92:316–31.
- Mason JM, Breitbart AS, Barcia M, Porti D, Pergolizzi RG, Grande DA. Cartilage and bone regeneration using gene-enhanced tissue engineering. *Clin Orthop* 2000;379S:S171–8.
- Issack PS, DiCesare PE. Recent advances toward the clinical application of bone morphogenetic proteins in bone and cartilage repair. *Am J Orthop* 2003;32:429–36.
- King GN. The importance of drug delivery to optimize the effect of bone morphogenetic proteins during periodontal regeneration. *Curr Pharm Biotechnol* 2001;2:131–42.
- Fiedler J, Roderer G, Gunther KP, Brenner RE. BMP-2, BMP-4, and PDGF-bb stimulate chemotactic migration of primary human mesenchymal progenitor cells. *J Cell Biochem* 2002;87:305–12.
- Postlethwaite AE, Raghov R, Stricklin G, Ballou L, Sampath TK. Osteogenic protein-1, a bone morphogenic protein member of the TGF-beta superfamily, shares chemotactic but not fibrogenic properties with TGF-beta. *J Cell Physiol* 1994;161:562–70.
- Muckle DS, Minns RJ. Biological response to woven carbon fibre pads in the knee: a clinical and experimental study. *J Bone Joint Surg Br* 1989;71:60–2.
- Buma P, Pieper JS, van Tienen T, van Susante JL, van der Kraan PM, Veerkamp JH, *et al.* Cross-linked type I and type II collagenous matrices for the repair of full-thickness articular cartilage defects—a study in rabbits. *Biomaterials* 2003;24:3255–63.
- Cohen SB, Meirisch CM, Wilson HA, Diduch DR. The use of absorbable co-polymer pads with alginate and cells for articular cartilage repair in rabbits. *Biomaterials* 2003;24:2653–60.
- Ushida T, Furukawa K, Toita K, Tateishi T. Three-dimensional seeding of chondrocytes encapsulated in collagen gel into PLLA scaffolds. *Cell Transplant* 2002;11:489–94.
- Chiroff RT, White RA, White EW, Weber JN, Roy D. The restoration of the articular surfaces overlying Replamineform porous biomaterials. *J Biomed Mater Res* 1977;11:165–78.
- Suominen E, Aho AJ, Vedel E, Kangasniemi I, Uusipaikka E, Yli-Urpo A. Subchondral bone and cartilage repair with bioactive glasses, hydroxyapatite, and hydroxyapatite-glass composite. *J Biomed Mater Res* 1996;32:543–51.
- Miyamoto S, Takaoka K, Okada T, Yoshikawa H, Hashimoto J, Suzuki S, *et al.* Evaluation of polylactic acid homopolymers as carriers for bone morphogenetic protein. *Clin Orthop* 1992;278:274–85.
- Saito N, Okada T, Horiuchi H, Murakami N, Takahashi J, Nawata M, *et al.* Biodegradable poly-D,L-lactide acid–polyethylene glycol blocks copolymers as a BMP delivery system for inducing bone. *J Bone Joint Surg Am* 2001;81-A:92–8.
- Saito N, Okada T, Horiuchi H, Murakami N, Takahashi J, Nawata M, *et al.* A biodegradable polymer as a cytokine delivery system for including bone formation. *Nat Biotechnol* 2001;19:332–5.
- Saito N, Okada T, Toba S, Miyamoto S, Takaoka K. New synthetic absorbable polymers as BMP carriers: plastic properties of poly-D,L-lactide acid–polyethylene glycol block copolymers. *J Biomed Mater Res* 1999;47:104–10.
- Tamai N, Myoui A, Tomita T, Nakase T, Tanaka J, Ochi T, *et al.* Novel hydroxyapatite ceramics with an interconnective porous structure exhibit superior osteoinduction *in vivo*. *J Biomed Mater Res* 2002;59:110–7.
- Nishikawa M, Myoui A, Ohgushi H, Ikeuchi M, Tamai N, Yoshikawa H. Bone tissue engineering using novel